










Distinct developmental phenotypes result from mutation of Set8/KMT5A and histone H4 lysine 20 in *Drosophila melanogaster*

Aaron T. Crain ^{1,2} Stephen Klusza ^{2,3,8} Robin L. Armstrong ^{1,2} Priscila Santa Rosa ⁴ Brenda R.S. Temple ^{2,5}
Brian D. Strahl ^{1,3,5} Daniel J. McKay ^{1,2,6,7} A. Gregory Matera ^{1,2,3,6,7,*} Robert J. Duronio ^{1,2,3,6,7,*}

¹Curriculum in Genetics and Molecular Biology, University of North Carolina, Chapel Hill, NC, 27599 USA,

²Integrative Program for Biological and Genome Sciences, University of North Carolina, Chapel Hill, NC, 27599 USA,

³Lineberger Comprehensive Cancer Center, University of North Carolina, Chapel Hill, NC, 27599 USA,

⁴UNC PREP, University of North Carolina, Chapel Hill, NC, 27599 USA,

⁵Department of Biochemistry and Biophysics, University of North Carolina, Chapel Hill, NC, 27599 USA,

⁶Department of Biology, University of North Carolina, Chapel Hill, NC, 27599 USA,

⁷Department of Genetics, University of North Carolina, Chapel Hill, NC, 27599 USA,

⁸Present address: Department of Biology, Clayton State University, Morrow, GA 30260 USA.

*Corresponding author: Integrative Program for Biological and Genome Sciences, University of North Carolina, Chapel Hill, NC, 27599 USA. Email: matera@unc.edu;

* Corresponding author: Integrative Program for Biological and Genome Sciences, University of North Carolina, Chapel Hill, NC, 27599 USA. Email: duroonio@med.unc.edu

Abstract

Mono-methylation of histone H4 lysine 20 (H4K20me1) is catalyzed by Set8/KMT5A and regulates numerous aspects of genome organization and function. Loss-of-function mutations in *Drosophila melanogaster* Set8 or mammalian KMT5A prevent H4K20me1 and disrupt development. Set8/KMT5A also has non-histone substrates, making it difficult to determine which developmental functions of Set8/KMT5A are attributable to H4K20me1 and which to other substrates or to non-catalytic roles. Here, we show that human KMT5A can functionally substitute for Set8 during *Drosophila* development and that the catalytic SET domains of the two enzymes are fully interchangeable. We also uncovered a role in eye development for the N-terminal domain of Set8 that cannot be complemented by human KMT5A. Whereas Set8^{20/20} null mutants are inviable, we found that an R634G mutation in Set8 predicted from *in vitro* experiments to ablate catalytic activity resulted in viable adults. Additionally, Set8(R634G) mutants retain significant, albeit reduced, H4K20me1, indicating that the R634G mutation does not eliminate catalytic activity *in vivo* and is functionally hypomorphic rather than null. Flies engineered to express only unmodifiable H4 histones (H4^{K20A}) can also complete development, but are phenotypically distinct from H4^{K20R}, Set8^{20/20} null, and Set8^{R634G} mutants. Taken together, our results demonstrate functional conservation of KMT5A and Set8 enzymes, as well as distinct roles for Set8 and H4K20me1 in *Drosophila* development.

Keywords: *Drosophila melanogaster*; Set8; H4K20me; development; histone modification; chromatin

Introduction

The formation of chromatin from DNA and histones regulates genome function and is critical for development of multicellular organisms. The post-translational modification (PTM) of histone N-terminal tails modulates the organization of chromatin and thereby helps regulate replication, repair, and transcription of the genome (Rothbart and Strahl 2014). Consequently, dysregulation of histone PTMs is thought to disrupt animal development. However, our understanding of how particular histone PTMs influence specific developmental processes is incomplete. For instance, methylation of histone H4 lysine 20 (H4K20me) has been implicated in the control of transcription (Karachentsev et al. 2005; Kalakonda et al. 2008; Wakabayashi et al. 2009; Abbas et al. 2010; Congdon et al. 2010; Brustel et al. 2011; Li et al. 2011a, 2011b, 2016; Yang et al. 2012; Beck et al. 2012b; Kapoor-Vazirani and Vertino 2014; Yao et al. 2014; Lv et al. 2016; Yu et al. 2019; Huang et al. 2021; Shoaib et al. 2018, 2021),

DNA replication and repair (Botuyan et al. 2006; Huen et al. 2008; Yin et al. 2008; Brustel et al. 2011; Beck et al. 2012b; Dulev et al. 2014; Hayashi-Takanaka et al. 2021), chromosome condensation during mitosis (Karachentsev et al. 2005; Centore et al. 2010; Brustel et al. 2011; Beck et al. 2012b), and heterochromatin assembly (Nishioka et al. 2002; Tardat et al. 2010; Brustel et al. 2011; Beck et al. 2012b; Shoaib et al. 2018). However, the requirement for these putative H4K20me functions has not been directly interrogated during animal development (McKay et al. 2015).

In most animal genomes, H4K20 monomethylation (H4K20me1) is catalyzed by a conserved enzyme variably termed KMT5A/Set8/SETD8/PR-Set7 that contains a catalytic SET domain (Fang et al. 2002; Nishioka et al. 2002). Subsequent di- and trimethylation of H4K20 is carried out by SET domain-containing Suv4-20 enzymes, of which there are two in mammals and one in *Drosophila* (Schotta et al. 2004; Sakaguchi et al.

Received: January 10, 2022. Accepted: March 28, 2022

© The Author(s) 2022. Published by Oxford University Press on behalf of Genetics Society of America. All rights reserved.

For permissions, please email: journals.permissions@oup.com

2008; Yang *et al.* 2008; Beck *et al.* 2012b; Weirich *et al.* 2016). Developmental roles for H4K20me are typically investigated by mutations that eliminate or alter the activity of these enzymes. Although most of this work has been performed using knock-down methods in cell culture (Julien and Herr 2004; Jørgensen *et al.* 2007; Tardat *et al.* 2007; Houston *et al.* 2008; Huen *et al.* 2008; Pannetier *et al.* 2008; Pesavento *et al.* 2008; Sims and Rice 2008; Wakabayashi *et al.* 2009; Abbas *et al.* 2010; Centore *et al.* 2010; Congdon *et al.* 2010; Oda *et al.* 2010; Tardat *et al.* 2010; Spektor *et al.* 2011; Sakaguchi *et al.* 2012; Yang *et al.* 2012; Beck *et al.* 2012a), a small number of studies were conducted using mutant animals (Fang *et al.* 2002; Karachentsev *et al.* 2005; Sakaguchi and Steward 2007; Schotta *et al.* 2008; Oda *et al.* 2009; Li *et al.* 2011b; Bateman *et al.* 2012). For instance, loss of the H4K20me2 methyltransferase Suv4-20h1 in mice causes early developmental defects, resulting in either embryonic or perinatal lethality (Schotta *et al.* 2008). In contrast, animals that lack the H4K20me3 methyltransferase Suv4-20h2 develop normally (Schotta *et al.* 2008). *Drosophila* Suv4-20 null mutations display no overt developmental defects, suggesting no essential requirement for H4K20me2 and H4K20me3 in flies (Sakaguchi *et al.* 2008). In contrast, loss of H4K20 monomethyltransferases causes severe developmental phenotypes: Fly Set8 (FlyBase annotation PR-Set7; CG3307) and mouse KMT5A null mutants are inviable and exhibit a developmental arrest that is accompanied by reduction of H4K20me and a variety of defects including smaller larval tissues in flies and increased apoptosis in mouse embryos (Karachentsev *et al.* 2005; Sakaguchi and Steward 2007; Huen *et al.* 2008; Oda *et al.* 2009). Mutant cells also have defects in cell cycle progression and accumulate DNA damage (Brustel *et al.* 2011; Wu and Rice 2011; Beck *et al.* 2012b). These cellular and developmental defects have been attributed to loss of downstream functions that require H4K20 methylation. Consistent with this interpretation, a KMT5A R265G mutation predicted to abolish catalytic activity does not support mouse embryonic development (Oda *et al.* 2009), suggesting that KMT5A catalytic activity is required for animal development.

Each of these analyses is confounded by observations that Set8 family enzymes have protein substrates in addition to H4K20 (Shi *et al.* 2007; Huen *et al.* 2008; Takawa *et al.* 2012; Dhami *et al.* 2013). Moreover, many of these other substrates, such as p53 and proliferating cell nuclear antigen (PCNA), regulate critical aspects of genome function (Shi *et al.* 2007; West *et al.* 2010; Takawa *et al.* 2012; Dhami *et al.* 2013). Finally, recent work from our group using engineered *Drosophila* histone mutant genotypes demonstrated that H4K20 is dispensable for DNA replication and organismal viability (McKay *et al.* 2015). Thus, the contributions of H4K20me to animal development are not fully determined.

Here, we compare phenotypes caused by mutation of Set8 and H4^{K20} in *Drosophila*. The data show that the essential function played by Set8 in fly development is not entirely dependent on its histone H4K20 methylation activity. We also demonstrate that human KMT5A can functionally substitute for loss of Set8 in *Drosophila*, indicating that flies can provide critical information about evolutionarily conserved functions of H4K20 monomethyltransferases during development.

Materials and methods

Fly stocks and husbandry

Fly stocks were maintained on standard corn medium with molasses provided by Archon Scientific (Durham). The Set8²⁰ stock used in this study was a generous gift from Ruth Steward. The

Set8¹ (#10278) stock was obtained from the Bloomington Stock Center.

Set8, KMT5A, and chimeric transgenes

For the Set8^{WT} transgene a 5,493-bp genomic fragment was amplified from a wild-type fly extract using the following primers 5' acttatacacttcctcct 3' and 5' taccgcctgatcggaatt 3'. The genomic fragment was cloned into pDEST w+ attB (Supplementary Fig. 2). Set8^{RG} and Set8^{RHLL} were constructed using the Q5 site-directed mutagenesis kit on pDEST w+ attB Set8^{WT} (NEB E0554S). KMT5A, Set8^{AN}, N-KMT5A::Set8-C, and N-Set8::KMT5A-C sequences were synthesized using GENEWIZ gene synthesis (Supplementary Fig. 3) and cloned into pDEST w+ attB digested with AgeI and MluI (Supplementary Fig. 2). Transgenes were sequence verified and injected into VK33 on chromosome 3L and screened for positive transformants by BestGene. Recombinant flies were generated by crossing transgenic flies with flies containing Set8²⁰ and screening single F2 male progeny for the presence of both the appropriate transgene and Set8²⁰.

Western blots

For Set8 western blots, 20 brains from third instar wandering larvae of each genotype were collected in 1×PBS (137 mM NaCl, 2.7 mM KCl, 10 mM Na₂HPO₄, 1.8 mM KH₂PO₄). 1×PBS was removed, 100 μl of RIPA buffer (50 mM Tris pH 7.5, 0.1% SDS, 0.5% sodium deoxycholate, 1% NP-40, 150 mM NaCl, 5 mM EDTA) was added to each sample. Larvae were homogenized in RIPA buffer using a pestle and incubated on ice for 30 min. Samples were then centrifuged for 15 min at top speed at 4°C. Supernatant was separated from pellet and protein concentration was assessed using a Bradford assay. Then 4× Laemmli sample buffer (BioRad 1610747) with 10% β-mercaptoethanol was added to each sample at a 3:1 ratio. Samples were boiled for 10 min and equal protein (~10 μg) was loaded on 12% SDS-PAGE gels. Proteins were transferred to a 0.45-nm nitrocellulose membrane for 60 min at 100 V. Membranes were blocked with 5% milk in 1×TBS-Tween (10 mM Tris, 150 mM NaCl, 0.1% Tween20) for 60 min then blotted with primary antibodies (Set8: Novus Biologicals 44710002; β-tubulin: Abcam ab6046) in 5% milk in 1×TBS-Tween overnight. Blots were quickly washed 3× then for 10 min 3×. Blots were incubated with goat anti-rabbit HRP secondary antibody (Chemicon) in 5% milk in 1×TBS-Tween for 2 h at room temperature, then again quickly washed 3× then for 10 min 3×. Blots were then incubated with SuperSignal West Pico PLUS Chemiluminescent Substrate (Thermo Scientific 34580) and imaged using a GE Amersham Imager. Quantification was performed using FIJI. Briefly, the signal of each band on the Set8 blot and β-tubulin blot was quantified using a box of equal area. Background was subtracted from each Set8 value, then divided by the corresponding background-subtracted β-tubulin signal for each lane. Finally, the value of Oregon-R was set to 1, so values of all other genotypes are relative to that genotype.

For H4K20me1 western blots, nuclei from 50 whole third instar wandering larvae from each genotype were collected as described previously (Penke *et al.* 2018; Leatham-Jensen *et al.* 2019). Nuclei were briefly resuspended in 1×PBS for protein quantification by Bradford assay. Then 4× Laemmli sample buffer (BioRad 1610747) with 10% β-mercaptoethanol was added to each sample at a 3:1 ratio. Samples were boiled for 10 min and sonicated using the Bioruptor Pico sonication system (Diagenode) for 10 cycles (10 min on, 10 min off). Equal protein (~5 μg) was loaded on 15% SDS-PAGE gels. Proteins were transferred to a 0.22-nm nitrocellulose membrane for 10 min at 100 V, then 20 min at 60 V.

Membranes were blocked with 5% milk in 1×TBS-Tween (10 mM Tris, 150 mM NaCl, 0.1% Tween20) for 60 min then blotted with primary antibodies (H4K20me1: Diagenode C15200147; Fibrillarin: Abcam Ab5821, pan H4: Abcam Ab10158, and pan H3 Abcam Ab1791) in 5% milk in 1×TBS-Tween overnight. Downstream washes and imaging were performed as above. Goat anti-mouse HRP secondary antibody (GE NA931V) was used for H4K20me1 blots and goat anti-rabbit HRP (Chemion) was used for Fibrillarin, pan H4, and pan H3. Quantification was performed using FIJI. Briefly, the signal of each band on the H4K20me1 blot and pan H4 blot was quantified using a box of equal area. Background was subtracted from each H4K20me1, then divided by the corresponding background-subtracted pan H4 signal for each lane. Finally, the value of Oregon-R was set to 1, so values of all other genotypes are relative to that genotype.

Viability assays

To investigate the requirement of Set8 and H4K20me for organismal viability, we enriched cultures of each genotype for first instar larvae by manually separating them from their wild-type siblings and monitored survival to pupal and adult developmental stages. All *His4r^{Δ/Δ}* genotypes in this study are *His4r^{15-4/15-4}*, except *H4^{K20A}*, *His4r^{Δ/Δ}* which is the *His4r* transheterozygote (*His4r^{15-4/59}*). Mean pupation and eclosion values and pairwise comparisons for all genotypes in this study can be found in Supplementary Table 3. Crosses to generate histone mutant genotypes were the same as reported previously (Meers et al. 2018b; Armstrong et al. 2019).

CRISPR for *His4r*

Two *His4rΔ* null alleles were utilized in this study. *His4r¹⁵⁻⁴* was generated by Armstrong et al. (2018). *His4r⁵⁹* is an additional CRISPR allele generated as in Armstrong et al. (2018) that results in a deletion of the same size as *His4r¹⁵⁻⁴*. Here we generated a point mutation allele (*His4r^{K20A}*) using CRISPR-Cas9 mutagenesis. The genomic region including *His4r* was amplified using the following primers 5'-gctgcgccgttagataaac-3' and 5'-agcaatcgagtc-catg-3' and TOPO cloned in pENTR. The codon for *His4r^{K20}* was changed to Ala using the Q5 Site-directed Mutagenesis kit (NEB E0554S). The same gRNA constructs in pCFD3 from Armstrong et al. (2018) were coinjected with the K20A-mutated *His4r* repair construct into *Drosophila* embryos expressing Cas9 from the *nanos* promoter. Positive hits were screened using a BbsI site created by the Lys to Ala mutagenesis.

Scanning electron microscopy

One- to three-day-old flies were dehydrated in ethanol and images of compound eyes were taken using a Hitachi TM4000Plus table top SEM microscope at 10 kV and 150× magnification. Total counts of penetrance included equal numbers of males and females because both displayed rough eyes. The numbers of flies scored are indicated by the denominators in each SEM figure. Expressivity varied amongst genotypes and was not quantified. The eye images shown in the figures are representative of the population for each genotype.

FACS

Wing imaginal disc nuclei from third instar wandering larvae of each genotype were sorted into G1, S, and G2 populations by a FACSaria II or III based on DAPI intensity as described previously (Meserve and Duronio 2017; Armstrong et al. 2018).

Protein sequence analyses

Figure 1a: PRDM and SET domain methyltransferase protein sequences (Supplementary Table 1) were compiled and aligned with ClustalOmega using the msa package (Bodenhofer et al. 2015). A distance matrix was calculated by identity using dist.alignment in the seqinr package. A phylogenetic tree based on the distance matrix was generated and then plotted using ggtree (Yu et al. 2017, 2018; Yu 2020).

Figure 2c: A BLAST search of the full-length *Drosophila melanogaster* Set8 protein sequence was performed against the refseq_protein database using the default parameters. The top 1,000 hits were compiled and manually sorted to include only one protein isoform per organism. Proteins with less than 50% identity to the full-length *D. melanogaster* Set8 were discarded. Human and mouse KMT5A proteins were retained for downstream analysis despite having percent identities lower than 50%. The remaining protein sequences (Supplementary Table 2) were aligned with ClustalOmega from the msa package (Bodenhofer et al. 2015). Phylogenetic classification of each protein was performed with the taxize package and merged with the alignment information (Chamberlain and Szöcs 2013). Proteins with incomplete classification information were discarded. A phylogenetic tree was generated using the classification information and plotted using ggtree (Yu et al. 2017, 2018; Yu 2020). The alignment of all remaining proteins was plotted in order of the phylogenetic tree and each position in the alignment was colored based on whether it matched the residue in the corresponding position of *D. melanogaster* Set8 (blue), Human KMT5A (pink), both *D. melanogaster* Set8 and KMT5A (maroon), or neither *D. melanogaster* Set8 and KMT5A (black). Gaps in the alignment are represented by white space.

Molecular dynamics simulations

Structural models of *Drosophila* WT and mutant Set8/KMT5A in ternary complexes with SAH (S-adenosyl-L-homocysteine) and H4 peptide were built using the crystallographic structure of human KMT5A in ternary complex (PDB ID: 1zkk) [PMID 15933070] as template. These structural models were then used as starting structures for molecular dynamics simulations. Four replicate explicit solvent simulations with the same starting conformations but different velocity distributions were completed for WT and each mutant using the Amber v18 software package (Case et al. 2018). LEaP from the Amber software package was used to generate the explicit solvent systems in an octahedral box with charge neutralization while the GPU version of PMEMD was used to complete the simulations (Götz et al. 2012; Salomon-Ferrer et al. 2013). The ff14SB force field was used for parameterization (Maier et al. 2015). A total of 5,000 steps of minimization were completed, followed by 500 ps heating with an NVT ensemble, and then density equilibration over 500 ps with an NPT ensemble. The production run was in the NPT ensemble for a total of 500 ns. During the production run, Langevin dynamics with a collision frequency of 1.0 ps⁻¹ was used for temperature regulation. A Berendsen barostat with a relaxation time of 1.0 ps was used for pressure regulation. The time-step was 2 fs with hydrogen atoms constrained by SHAKE. Trajectories were analyzed for the distance between atoms in Set8/KMT5A and atoms in either the H4 peptide or SAH.

Full genotypes of strains used in this study

Set8^{WT}: y-w-;;{Set8^{WT}}, Set8^{20/20}
 Set8^{RG}: y-w-;;{Set8^{RG}}, Set8^{20/20}

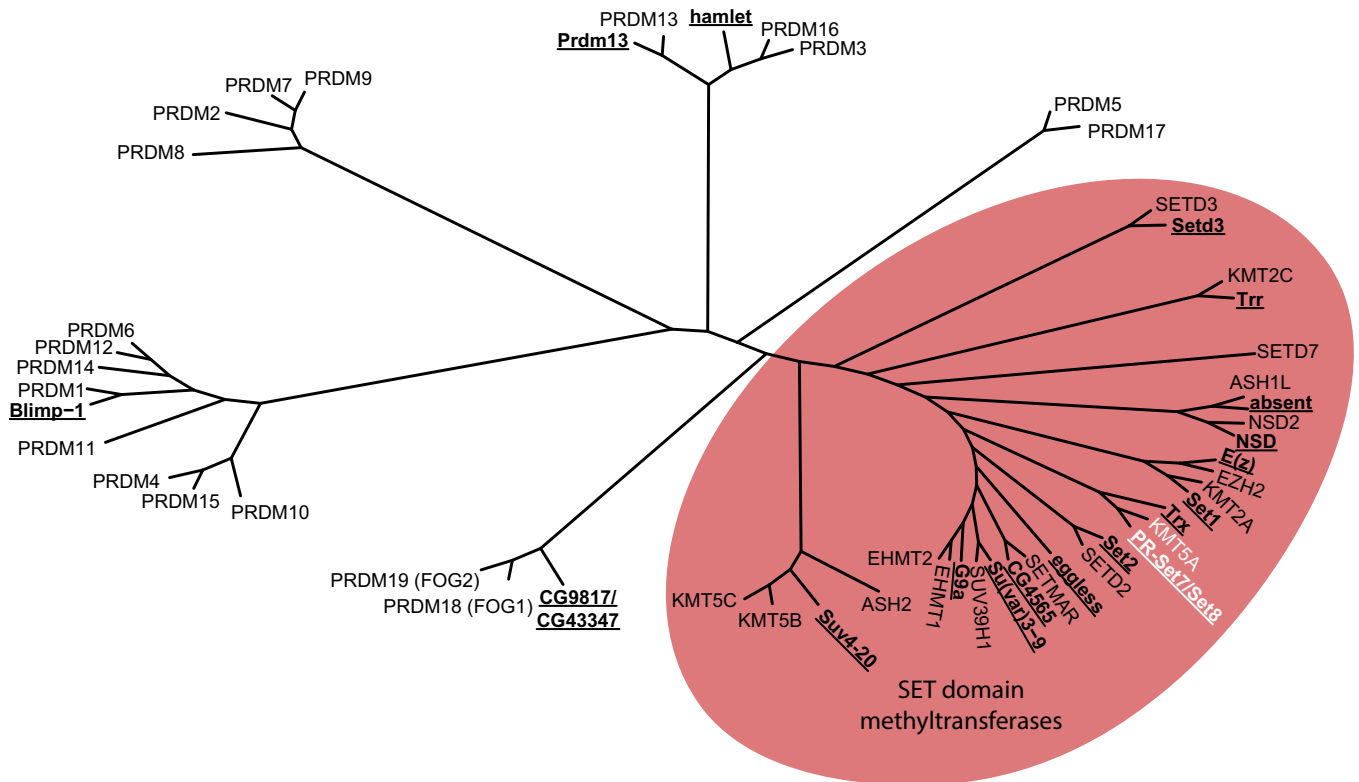


Fig. 1. Evolutionary relationship of *Drosophila* and human SET and PRDM-containing proteins. Unrooted tree produced from an alignment of human and *Drosophila* PRDM and SET domain family proteins using ClustalOmega. *Drosophila* proteins are indicated with bold, underlined text. The oval highlights the grouping of SET domain family proteins, including PR-Set7/Set8 and KMT5A (white text).

Set8^{R^{GHL}}: y-w-;;{Set8^{R^{GHL}}}, Set8^{20/20}
 KMT5A: y-w-;;{KMT5A}, Set8^{20/20}
 Set8^{ΔN}: y-w-;;{Set8^{Δ1-339}}, Set8^{20/20}
 N-KMT5A::Set8-C: y-w-;;{KMT5A¹⁻²¹⁴::Set8⁵⁵⁵⁻⁶⁹¹}, Set8^{20/20}
 N-Set8::KMT5A-C: y-w-;;{Set8¹⁻⁵⁵⁴::KMT5A²¹⁵⁻³⁵²}, Set8^{20/20}
 HWT: y-w-; ΔHisC; {12xHWT}
 HWT, His4r^{ΔA}: y-w-; ΔHisC; {12xHWT}, His4r^{15-4/15-4}
 H4^{K20A}: y-w-; ΔHisC; {12xH4^{K20A}}
 H4^{K20R}: y-w-; ΔHisC; {12xH4^{K20R}}
 H4^{K20A}, His4r^{ΔA}: y-w-; ΔHisC; {12xH4^{K20A}}, His4r^{15-4/S9}
 H4^{K20A}, His4r^{K20A/Δ}: y-w-; ΔHisC; {12xH4^{K20A}}, His4r^{K20A/15-4}
 H4^{K20R}, His4r^{ΔA}: y-w-; ΔHisC; {12xH4^{K20R}}, His4r^{15-4/15-4}

Results

Set8 is the appropriate designation for the *Drosophila* H4K20 mono-methyltransferase

The *D. melanogaster* genome encodes 14 SET [Su(var)3-9, Enhancer-of-zeste, Trithorax] domain lysine methyltransferases (FlyBase) (Schotta et al. 2004; Dillon et al. 2005; Mis et al. 2006; Mohan et al. 2011; Shilatifard 2012; Jiang et al. 2017) (Fig. 1 and Supplementary Table 1). A related family of proteins, called PRDMs, is characterized by the presence of a PR domain [PRDF1 (positive regulatory domain I-binding factor 1) and RIZ1 (retinoblastoma protein-interacting zinc finger gene 1)] along with a variable number of Cys2-His2 (C2H2) zinc fingers (Tullio et al. 2021). The PR domain is an evolutionarily recent subtype of the SET domain, although not all PRDMs encode active methyltransferases (Tullio et al. 2021). There are four PRDM proteins (Blimp-1, Hamlet, CG43347, Prdm13) in insect genomes whereas this family

has expanded to 19 proteins in humans (Fumasoni et al. 2007; Manes et al. 2017; Tullio et al. 2021).

In *Drosophila*, the protein encoded by PR-Set7/CG3307 is orthologous to the human H4K20 methyltransferase SETD8/KMT5A and it neither contains a PR domain nor any predicted zinc finger motifs (Fang et al. 2002; Nishioka et al. 2002; Brustel et al. 2011) (Fig. 1, Supplementary Fig. 1). In contrast, human PRDM7 (PR/SET Domain 7) is an H3K4 methyltransferase that is most closely related to the KRAB and Zn finger domain protein, PRDM9 (Blazer et al. 2016) (Fig. 1). Moreover, human SETD7/Set7/Set9 is yet another human H3K4 methyltransferase (Wang et al. 2001) distinct from *Drosophila* PR-Set7/CG3307 (Fig. 1). To avoid further confusion, we propose to officially rename CG3307 as Set8 and refer to this protein as Set8 throughout the manuscript.

Human KMT5A rescues loss of Set8 in *Drosophila*

KMT5A and Set8 are essential for the development of mice and flies, respectively, and mutating these enzymes results in defects in cell cycle progression, DNA damage response, and chromatin compaction in both organisms (Karachentsev et al. 2005; Oda et al. 2009; Sakaguchi et al. 2012). The SET domains of Set8 and human KMT5A share 57% identical amino acids (with 72% conserved) (Supplementary Fig. 1). Therefore, we hypothesized that KMT5A and Set8 perform the same biological functions in *Drosophila* and mammals and that human KMT5A would rescue loss of Set8 in *Drosophila*. To test this hypothesis, we engineered a KMT5A open reading frame that was codon optimized for translation in *Drosophila* and expressed in the context of the native Set8 gene (a 4,774-bp genomic fragment including 1,325-bp upstream of the ORF and 2,021-bp downstream of the ORF including both native 5' and 3' UTRs) (Supplementary Figs. 2 and 3). Using this

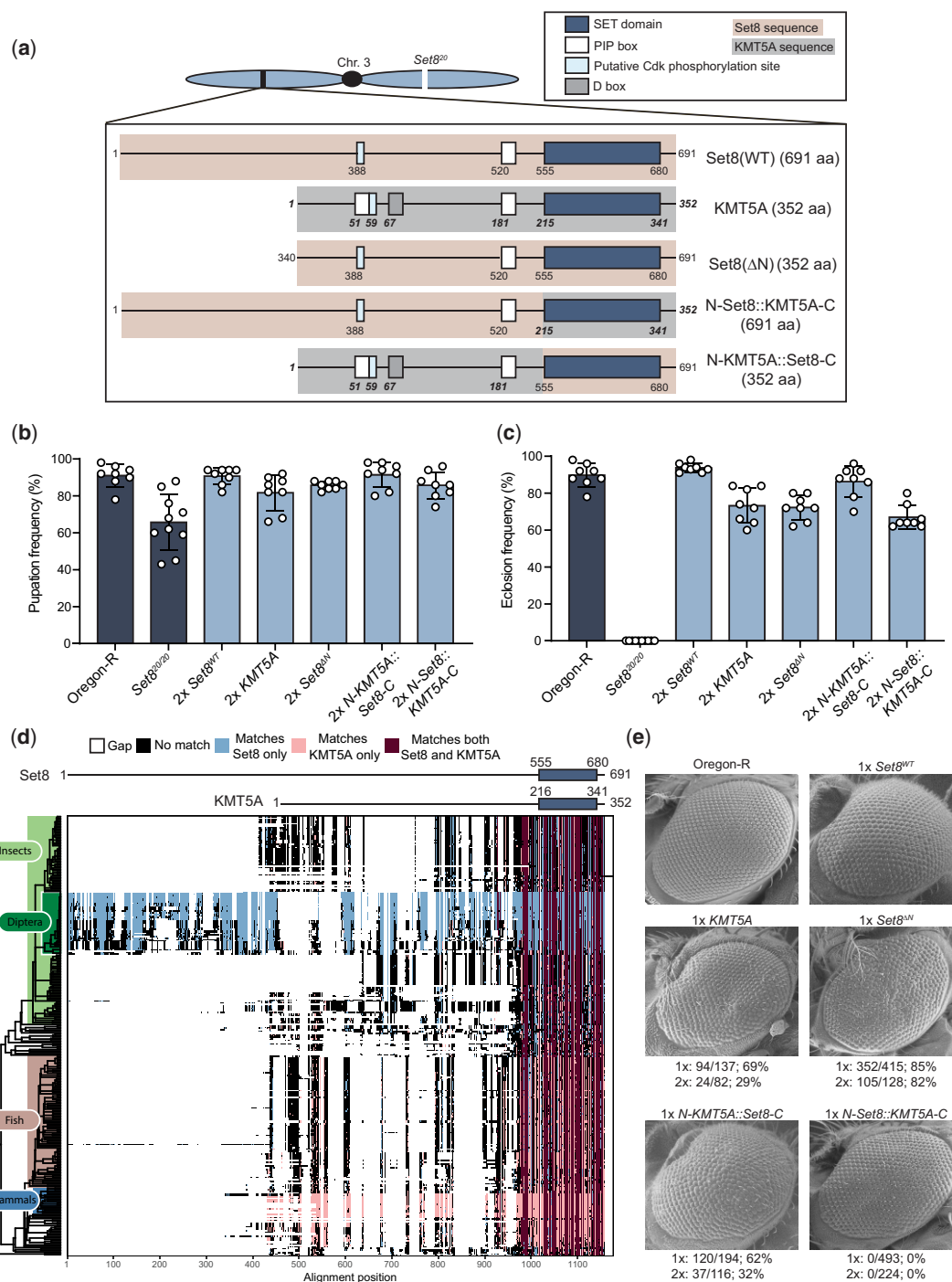


Fig. 2. Human KMT5A functionally substitutes for Set8 during *Drosophila* development. a) Diagram of Set8, KMT5A, and Set8/KMT5A chimeric proteins expressed from transgenes located on chromosome 3, which also contains the *Set8²⁰* null allele. Red shading and nonbold, nonitalic numbers indicate Set8 sequence. Gray shading and bold, italic numbers indicate KMT5A sequence. In parentheses is the total number of amino acids in each protein product. b) Pupation of *Set8^{WT}*, KMT5A, and chimera genotypes. Each circle represents the percentage of 40–50 larvae in a vial that reached pupation. The mean and standard deviation of these percentages for 8–10 vials are shown for the indicated genotypes. All transgenic genotypes are in the *Set8^{20/20}* homozygous null background. “2x” indicates that each transgene is also homozygous. Significance was determined by a one-way ANOVA followed by Tukey’s multiple comparison test. P-values for pairwise comparisons can be found in Table 1 and Supplementary Table 3. c) Eclosion into adults of *Set8^{WT}*, KMT5A, and chimera genotypes. Here, each circle represents a vial of 40–50 larvae, and 8 vials for each of the indicated genotypes were scored. Genotypes are as in panel B. Significance was determined by a one-way ANOVA followed by Tukey’s multiple comparison test. P-values for pairwise comparisons can be found in Table 1 and Supplementary Table 3. d) Annotated alignment of Set8-related proteins. A total of 301 homologous proteins with over 50% identity to Set8 as identified via BLAST were aligned using Clustal Omega and ordered by phylogeny. Set8 and KMT5A schematics are shown at the top of the diagram with the SET domains indicated by dark blue boxes. Residues of each protein in the alignment that match both Set8 and KMT5A exactly are colored dark red. Those that match only Set8 are colored light blue, and those that match only KMT5A are colored pink. Residues that match neither are colored black. Gaps in the alignment are indicated by white space. e) SEM images of adult eyes of flies of the indicated genotypes. The penetrance of flies displaying a phenotype like that shown is indicated below each image. Both males and females were included in the penetrance calculation. “1x” and “2x” indicate flies containing either 1 or 2 copies, respectively, of the transgene expressing Set8, KMT5A, or Set8/KMT5A chimeras in the *Set8^{20/20}* homozygous null background.

Table 1 Pairwise comparisons of pupation and eclosion frequencies among *Set8*^{WT}, *KMT5A*, and *Set8/KMT5A* chimera genotypes

Genotype	Pupation frequency (%)	Eclosion frequency (%)		1	2	3	4	5	6
Oregon-R	0.91	0.90	1		****	ns	**	ns	****
<i>Set8</i> ^{20/20}	0.66	0.00	2	****		****	****	****	****
2x <i>Set8</i> ^{WT}	0.91	0.94	3	ns	****		****	ns	****
2x <i>KMT5A</i>	0.82	0.74	4	ns	*	ns		ns	ns
2x N- <i>KMT5A</i> :: <i>Set8</i> -C	0.91	0.86	5	ns	****	ns	ns		****
2x N- <i>Set8</i> :: <i>KMT5A</i> -C	0.86	0.67	6	ns	***	ns	ns	ns	

Dark gray = pupation, light gray = eclosion.

**** P < 0.0001,

*** P < 0.001,

** P < 0.01,

* P < 0.05,

ns = not significant.

engineered *KMT5A* allele and a wild-type *Set8* allele (hereafter *Set8*^{WT}), we generated transgenes located on the same chromosome as the *Set8*²⁰ null allele (Karachentsev et al. 2005) (Fig. 2a). Whereas *Set8*^{20/20} mutants die as early pupae, animals expressing *KMT5A* in a *Set8*^{20/20} background pupate normally and complete development at similar frequencies as wild-type animals or *Set8*^{20/20} animals rescued with a control *Set8*^{WT} transgene (Fig. 2, b and c and Table 1). Although *Set8*^{20/20} animals rescued by *KMT5A* are viable and capable of producing offspring, we observed a rough eye phenotype in 69% or 29% of adult flies containing one or two copies, respectively, of the *KMT5A* transgene (Fig. 2e). The *Drosophila* compound eye is a highly organized tissue containing ~800 photoreception structures termed ommatidia, each composed of eight photoreceptor neurons and a set of accessory cells. Many processes contribute to proper formation of the adult eye, including cell cycle progression, cell death, and ultimately cell differentiation. Disruption of any one of these processes can contribute to ommatidial irregularities that manifest as a visible “roughness” of the adult eye (Wolff and Ready 1991; Baker et al. 2014). Even subtle defects in gene functions required for eye development can result in rough eyes, and thus we conclude that *KMT5A* fully rescues most, but not all, *Set8* functions in *Drosophila*.

The N-terminus of *Set8* is dispensable for *Drosophila* viability but plays a role in eye development

Although the SET domains of *Set8* and *KMT5A* are 57% identical, the full-length proteins are only 21% identical (Supplementary Fig. 1). The N-terminal region (554aa) of *Set8* is predicted to be largely unstructured and is not well-conserved with *KMT5A* (Fig. 2a). A multiple protein alignment of 301 BLAST hits with greater than 50% identity to the full-length *Set8* protein revealed that this N-terminal region of *Set8* is unique to flies (order Diptera), whereas the SET domain is highly conserved across all represented organisms (Fig. 2d and Supplementary Table 2). To test whether the N-terminal region of *Set8* is necessary for *Drosophila* development, we engineered a transgene encoding a *Set8* protein lacking the first 339 amino acids (*Set8*^{AN}), which would produce a protein the size of *KMT5A* (Fig. 2a and Supplementary Figs. 2 and 3). The *Set8*^{AN} allele retains regulatory sequences including the PIP degen beginning at residue 517 (Jørgensen et al. 2007; Zouaz et al. 2018) and a putative Cdk phosphorylation site at residues 388–391. Because nothing is known about the N-terminal region and no other motifs are identifiable upstream of residue 388, we made the semi-arbitrary decision to create a truncated *Set8* protein that begins at residue 340 and thus would be of equal size to human *KMT5A* (Fig. 2a and

Supplementary Figs. 2 and 3). The *Set8*^{AN} transgene rescued *Set8*^{20/20} lethality resulting in viable, fertile adults with a highly penetrant (82%) rough eye phenotype (Fig. 2, b, c, and e). Although we were unable to assess the protein accumulation of *Set8*(Δ N) because the epitope recognized by the *Set8* antibody is within the N-terminal region, these results indicate that the N-terminal 339 amino acids are dispensable for normal development except in the eye. To test whether the eye function could be provided by *KMT5A*, we generated a chimeric transgene with the *Set8* N-terminus (1–554) fused to the *KMT5A* C-terminus (N-*Set8*::*KMT5A*-C) and a reciprocal chimeric transgene with the *KMT5A* N-terminus (1–214) fused to the *Set8* C-terminus (N-*KMT5A*::*Set8*-C). Both transgenes fully rescued viability and fertility of *Set8*^{20/20} mutants (Fig. 2, b and c). Further, N-*KMT5A*::*Set8*-C animals displayed a rough eye phenotype like *KMT5A* and *Set8*^{AN} animals (Fig. 2e). By contrast, flies expressing the N-*Set8*::*KMT5A*-C chimera were fully viable and fertile with morphologically normal eyes, indicating the human *KMT5A* SET domain is functionally equivalent to that from *Drosophila* *Set8* (Fig. 2, b and c). We conclude that the N-terminal 339 amino acids of *Set8* are dispensable for *Drosophila* viability and fertility but have a function in eye development that cannot be provided by the first 214 amino acids of human *KMT5A*.

A SET domain mutation predicted to block methyltransferase activity does not result in a *Set8* null phenotype

Many of the established roles for the *KMT5A/Set8* lysine methyltransferase have been attributed to its catalytic activity, primarily by using cell culture-based assays (Julien and Herr 2004; Jørgensen et al. 2007; Tardat et al. 2007; Houston et al. 2008; Huen et al. 2008; Pannetier et al. 2008; Pesavento et al. 2008; Sims and Rice 2008; Wakabayashi et al. 2009; Abbas et al. 2010; Centore et al. 2010; Congdon et al. 2010; Oda et al. 2010; Tardat et al. 2010; Spektor et al. 2011; Sakaguchi et al. 2012; Yang et al. 2012; Beck et al. 2012a). SET domains are highly conserved and contain evolutionarily invariant residues within the catalytic core (Fig. 3a). As shown in Fig. 3b, two of these residues (R634 and H638 in fly *Set8*) make critical contacts with the enzyme cofactor, S-adenosyl homocysteine (SAH). Note that SAH was used to generate the original crystal structure rather than the native methyl donor, S-adenosyl methionine (Couture et al. 2005). Mutation of the homologous Arg residue in the human enzyme (R265) to Gly blocks methyltransferase activity *in vitro* using nucleosomal substrates, and this substitution has been used in numerous studies of *Set8/KMT5A* proteins to create catalytically inactive enzymes (Nishioka et al. 2002; Shi et al. 2007; Tardat et al. 2007; Houston et al. 2008; Kalakonda et al. 2008; Sims and Rice 2008; Oda et al.

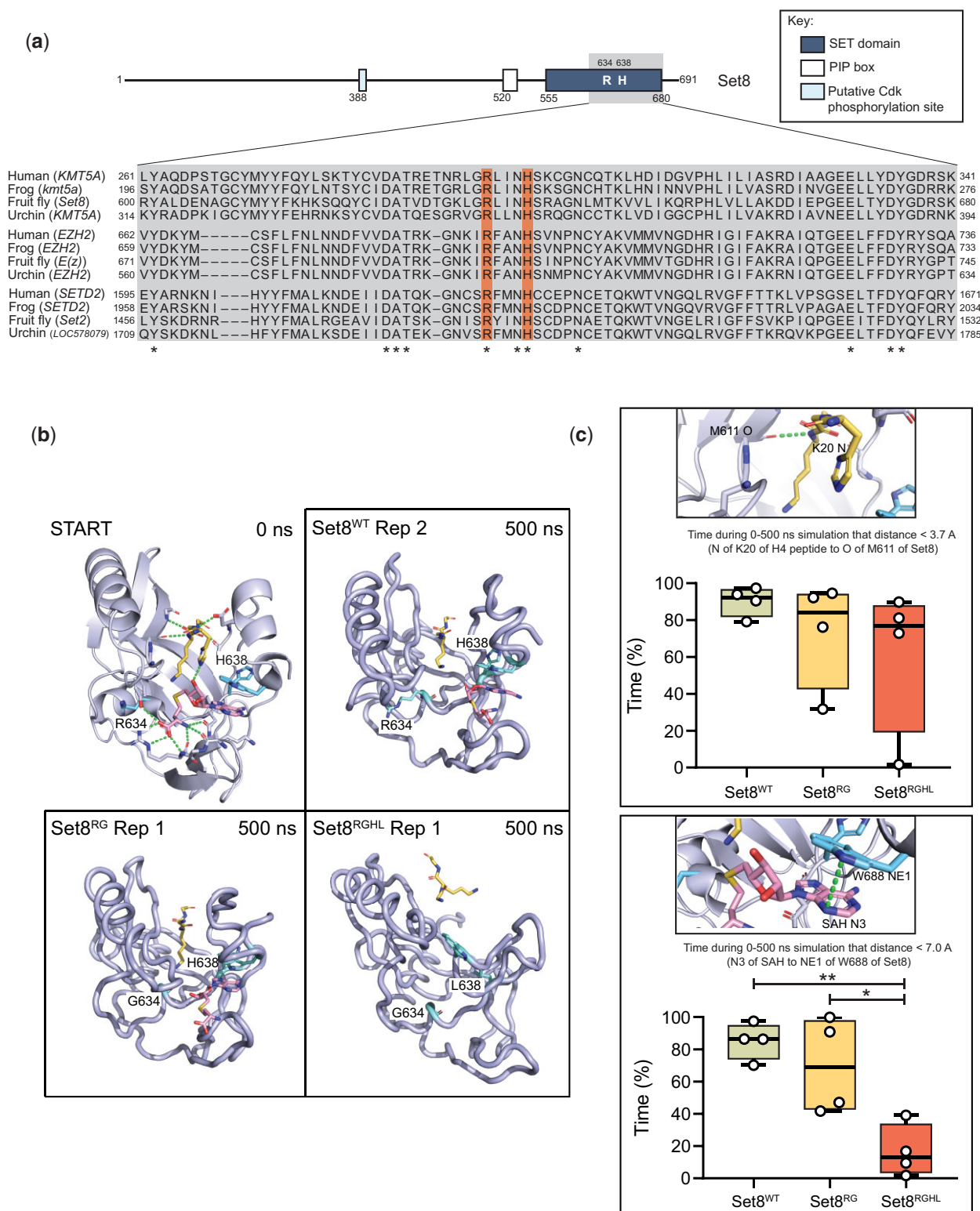


Fig. 3. Generation Set8 proteins predicted to be catalytically inactive. a) Diagram of Set8 and conservation of the Set8 Arg634 and Leu638 residues (orange bars) among KMT5A proteins from human, frog, and sea urchin, and among other SET domain proteins from these species. Gray inset indicates region of Set8 SET domain shown in alignment. Numbers on the left and right of the gray box indicate the starting and ending amino acid positions for each protein sequence. Asterisks mark where residues are identical across all 12 proteins. b) Modeling of Set8 with SAH and peptide from H4 bound to the enzyme. Shown are representative structures after 500 ns of molecular dynamics for Set8, Arg634Gly and Arg634Gly, His638Leu mutations in Set8. Ending structures for all replicates can be found in Supplementary Fig. 4. The 10-residue H4 peptide (A-K-R-H-R-K₂₀-V-L-R-D) is yellow, SAH is magenta, and the R/G634 and H/L638 amino acid side chains are cyan. c) Total length of time during 500 ns simulations that ligands remained in binding pocket as measured by distances between key atoms. The two distance measurements shown were selected because they were the most stable interactions between Set8 and H4 peptide and between Set8 and SAH. The selected hydrogen bond to the peptide was also the most stable interaction with the peptide and one of the last to be broken. Circles represent values from four replicate simulations. Significance was determined by a one-way ANOVA followed by Tukey's multiple comparison test. * indicates $P < 0.05$, ** indicates $P < 0.01$, and all other comparisons are not significant.

2009; Abbas et al. 2010; Congdon et al. 2010; Tardat et al. 2010; Wu et al. 2010; Abbas et al. 2013; Dulev et al. 2014). Using in silico structural models based on the solved human KMT5A structure and molecular dynamics simulations (Fig. 3b, Supplementary Fig. 4), each of these amino acid changes were evaluated for their impact on SAH binding and H4 peptide binding. While H4 peptide binding was minimally impacted, the mutations were shown to disrupt SAH binding and thus are predicted to reduce or eliminate methyltransferase activity of the mutant Set8 proteins (Fig. 3, b and c).

To determine whether methyltransferase activity is required for Set8 function during *Drosophila* development, we analyzed mutations in the SET domain that are predicted to ablate catalytic activity (Fang et al. 2002; Nishioka et al. 2002). We introduced R634G single (hereafter Set8^{RG}) and R634G, H638L double (hereafter Set8^{RGHL}) mutations in the context of the rescuing Set8^{WT} construct and generated transgenes at the same chromosomal landing site used for the KMT5A rescue experiments (Fig. 4a). We assessed expression of these transgenes in a Set8^{20/20} background by immunoblot analysis of third instar larval brain extracts (Fig. 4b and Supplementary Fig. 5). As demonstrated previously, there is no detectable Set8 protein in Set8^{20/20} homozygous null mutant animals (Karachentsev et al. 2005) (Fig. 4, b and c). The Set8(RGHL) mutant protein accumulates to about 10% of Oregon-R wild-type control (Fig. 4, b and c), suggesting that binding of the SAM cofactor stabilizes Set8 protein. Set8^{RGHL} animals are phenotypically similar to Set8^{20/20} null mutants, arresting development as early pupae (Fig. 5, a and b). Interestingly, Set8^{RGHL} wandering larvae accumulate melanotic masses that we rarely observe in Set8^{20/20} animals (Fig. 5c). This phenotype is associated with immune response and was previously reported to be variably expressive and penetrant in both Set8²⁰ and Set8^{1/Df(3R)red3l} animals (Minakhina and Steward 2006). In contrast, levels of the Set8(RG) missense protein are comparable to those of wild-type Set8 expressed from a control Set8^{WT} transgene (Fig. 4, b and c), indicating that the R634G mutation does not impact protein stability. The Set8^{RG} transgene rescues the early pupal lethality observed in Set8^{20/20} mutants, but only ~50% of the Set8^{RG} animals eclose as adults compared to the Set8^{WT} control (Fig. 5, a and b and Table 2). A majority of Set8^{RG} mutant flies had rough eyes (86%, Fig. 5d), as was previously shown for flies harboring the Set8¹ hypomorphic mutation, which is caused by a P-element insertion in the 5'-UTR (Fang et al. 2002; Nishioka et al. 2002; Karachentsev et al. 2005). Set8^{RG} also behaves as a hypomorphic allele, as animals containing two Set8^{RG} transgenes have a less severe phenotype than those containing one (Fig. 5b).

Given that the Set8^{RG} allele behaves as a genetic hypomorph, we asked whether the Set8(RG) mutant enzyme was catalytically active by assessing H4K20me1 levels in Set8^{RG} larvae by western blot (Fig. 4d and Supplementary Fig. 6). In contrast to previous in vitro evidence predicting that Set8(RG) would be catalytically inactive (Fang et al. 2002; Nishioka et al. 2002), Set8^{RG} mutants have about half of the H4K20me1 as control (Fig. 4, d and e). We interpret this result to indicate that Set8(RG) is impaired, but not inactive, for H4K20 methyltransferase activity *in vivo*, consistent with our genetic data. Curiously, we also found that H4 levels consistently appeared decreased relative to Fibrillarin and H3 in Set8^{20/20} and Set8^{RGHL} mutants, although this decrease did not become statistically significant because of high variability when using the anti-H4 antibody (Supplementary Fig. 7). We do not know the basis for this observation, but it may suggest a role for H4K20 methylation in H4 protein accumulation or stability, or an inability to efficiently recover unmethylated H4 protein from

chromatin using our extraction conditions. Nevertheless, these data indicate that the Set8^{RG} allele is not null, and that Set8(RG) protein retains some H4K20me1 activity *in vivo*.

To further characterize the Set8^{RG} mutant, we more closely evaluated the process of pupariation in our collection of Set8 mutants. Easily recognizable developmental events occur during the larval to pupal transition in *Drosophila*, including eversion of the anterior spiracles and gas bubble translocation from the posterior to anterior end of the pupa. Whereas Set8^{+/20} heterozygotes and Set8^{1/20} hypomorphs progress normally through these developmental milestones, Set8^{20/20} mutants fail to complete both anterior spiracle eversion and gas bubble translocation (Fig. 5f), resulting in pupae with increased length compared to control and Set8^{1/20} hypomorphs (Fig. 5e). Set8^{RG} animals displayed a slight defect in completion of these pupariation events compared to Set8^{WT} control animals (Fig. 5f). Pupariation defects observed in Set8^{RGHL} animals were like those in Set8^{20/20} mutants (Fig. 5f). Interestingly, Set8^{RG} mutants also displayed a slight increase in pupal length compared to Set8^{WT} controls that did not reach the severity observed in Set8^{20/20} mutants (Fig. 5e). These data demonstrate that the SET catalytic domain mutant Set8^{RG} displays intermediate pupariation defects between wild-type and null alleles of Set8, consistent with it being functionally hypomorphic.

Mutants of H4^{K20} and Set8 are phenotypically distinct

Mutation of lysine methyltransferases can result in disruption of multiprotein complexes, causing pleiotropic phenotypes independent of histone methylation (Zhang et al. 2015; Thandapani et al. 2017; Hamidi et al. 2018; Cornett et al. 2019; Lukinović et al. 2020; Sugeedha et al. 2021). In addition, Set8 has non-histone substrates and non-catalytic functions (Shi et al. 2007; Huen et al. 2008; Sims and Rice 2008; Yin et al. 2008; Takawa et al. 2012; Dhami et al. 2013; Dulev et al. 2014; Zouaz et al. 2018). Thus, one cannot conclusively determine functional roles for H4K20me solely by mutating Set8. Another genetic strategy to address the contribution of H4K20me to various genomic processes is to change H4^{K20} to a residue that cannot be modified by Set8. However, this genetic strategy is not usually employed in metazoan systems because in these organisms the replication-dependent (RD) histones (H1, H2A, H2B, H3, and H4) are encoded by multiple genes located at different loci, making genetic manipulation extremely difficult. In contrast, in *D. melanogaster* all ~100 RD histone genes are tandemly arrayed at a single locus that can be removed with a single genetic deletion (Δ His^C, Günesdogan et al. 2010). The early developmental arrest caused by homozygosity of this deletion can be rescued with a single, ectopic transgene encoding 12 tandemly arrayed histone wild-type gene repeats (HWT; Fig. 6a, see Meers et al. 2018b for details on array construction). This strategy allows us to engineer histone genotypes encoding mutant histone proteins in which a given residue is changed to one that is not a substrate for its cognate modifying enzyme (McKay et al. 2015; Penke et al. 2016; Meers et al. 2017; Armstrong et al. 2018; Penke et al. 2018; Meers et al. 2018a,b; Leatham-Jensen et al. 2019).

Using this strategy, we demonstrated previously that H4^{K20A} mutant animals can survive to adulthood (McKay et al. 2015) (Fig. 6, b and c). By contrast, 100% of Set8^{20/20} null animals die as larvae or early pupae (Karachentsev et al. 2005) (Fig. 2c). This stark phenotypic difference between H4^{K20A} and Set8 mutants suggests that certain Set8 phenotypes might not be due to loss of H4K20me, but rather to loss of methylation of non-histone substrates or non-catalytic functions of Set8. To investigate this

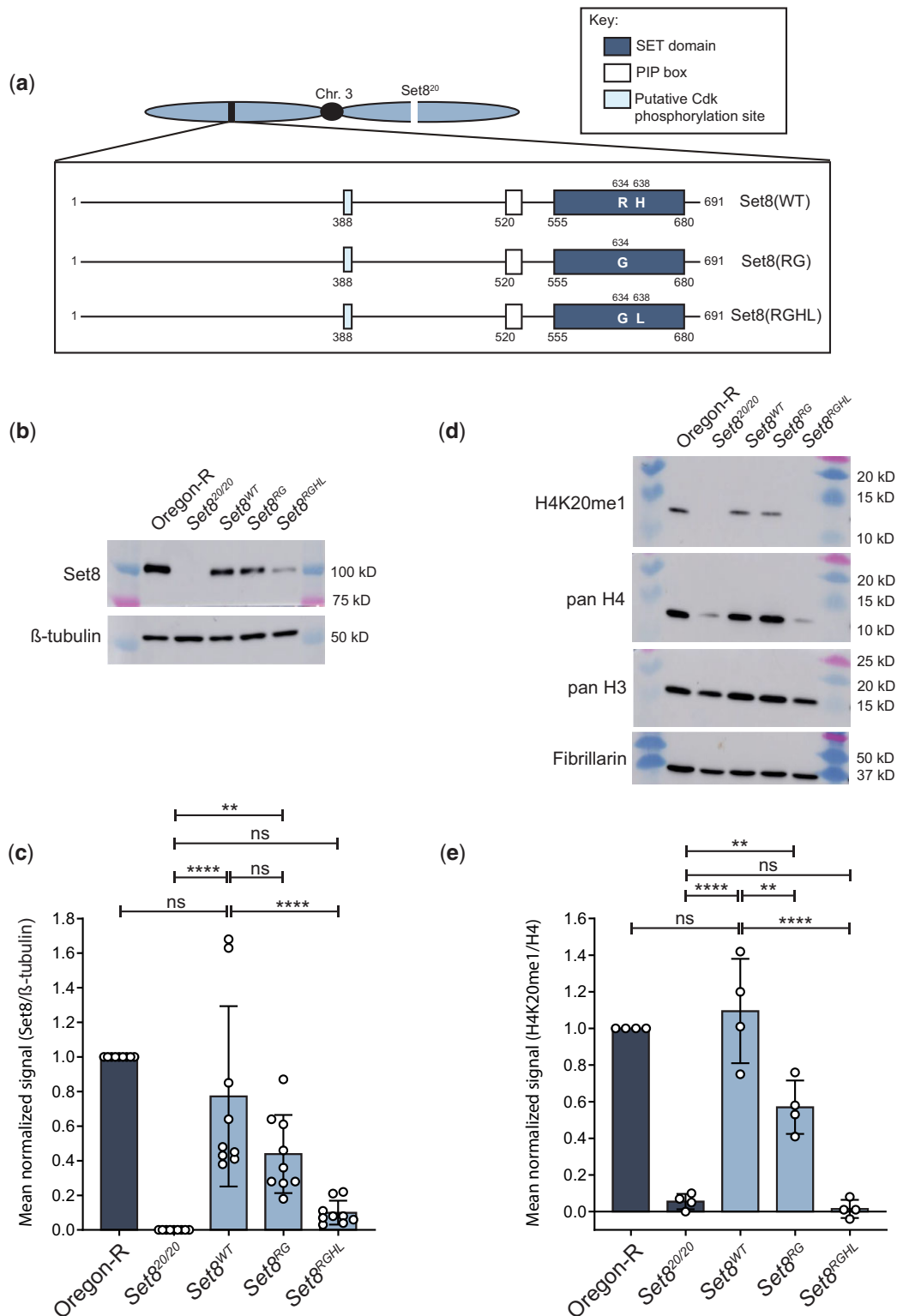
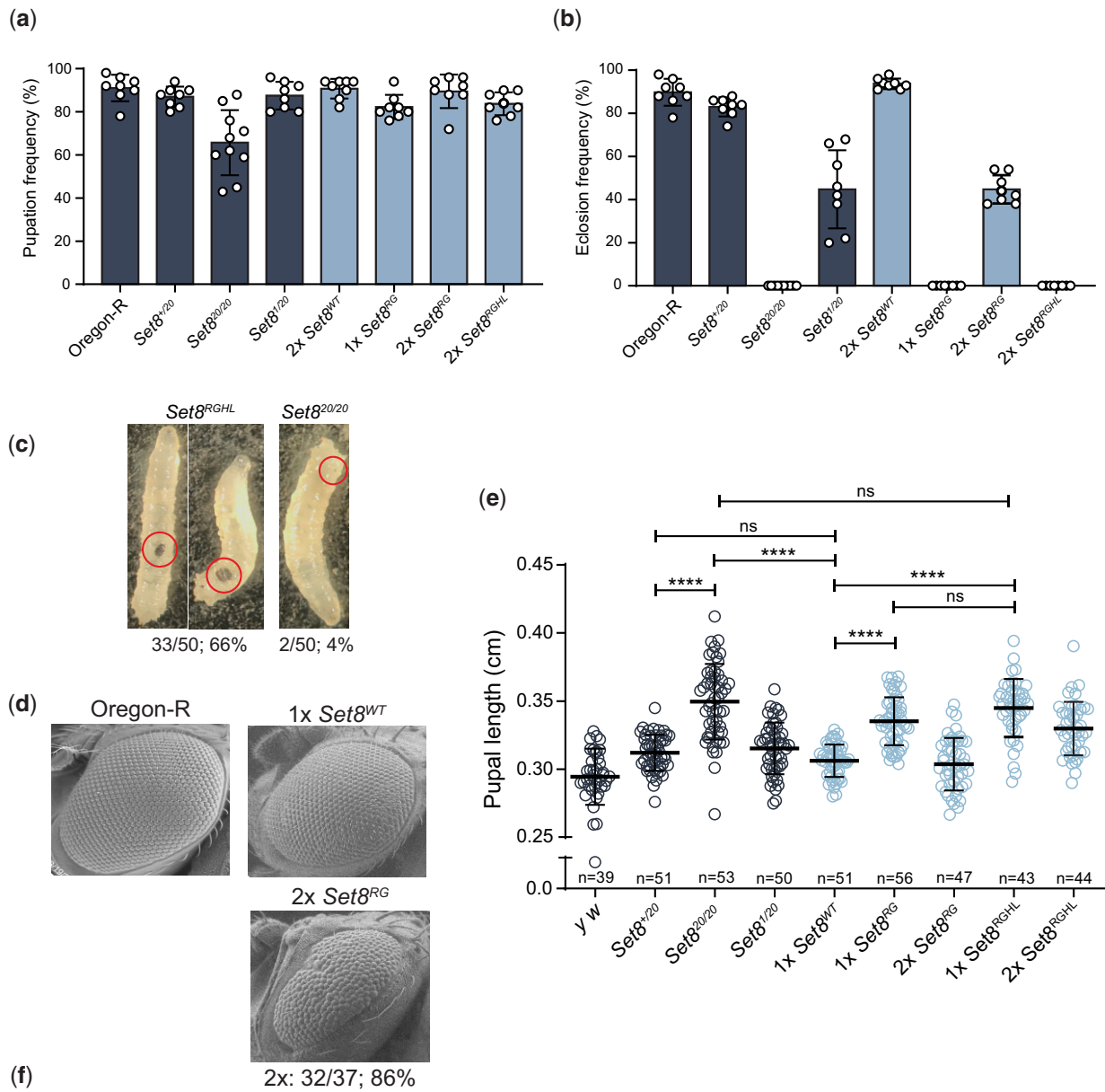


Fig. 4. Set8(RG) mutant enzyme retains H4K20me1 in vivo. a) Diagram of Set8(WT), Set8(RG), and Set8(RGHL) proteins expressed from transgenes located on chromosome 3. b) Western blot of third instar larval brain extracts from Oregon-R wild-type and the indicated Set8 mutants using anti-Set8 and anti-β-tubulin antibodies. For uncropped membrane images, see Supplementary Fig. 5. c) Quantification of anti-Set8 signal on western blots by densitometry (see Materials and methods). Shown is the mean and standard deviation of measurements (circles) from technical replicates across four biological replicates. Oregon-R normalized signal was set to 1 for each replicate. Significance was determined by a one-way ANOVA followed by Tukey's multiple comparison test. ** indicates $P < 0.01$, **** indicates $P < 0.0001$, and ns indicates not significant. d) Western blot of third instar larval nuclear extracts from Oregon-R wild-type and the indicated Set8 mutants using anti-H4K20me1, anti-pan H4, anti-pan H3, and anti-Fibrillarin antibodies. For uncropped membrane images see Supplementary Fig. 6. e) Quantification of anti-H4K20me1 signal on western blots by densitometry (see Materials and methods). Shown is the mean and standard deviation of measurements (circles) across three biological replicates normalized to pan H4 signal. Oregon-R normalized signal was set to 1 for each replicate. Significance was determined by a one-way ANOVA followed by Tukey's multiple comparison test. ** indicates $P < 0.01$, **** indicates $P < 0.0001$, and ns indicates not significant.



Genotype	Total pupae scored	Anterior spiracle eversion		Gas bubble translocation	
		# Completed	% Completed	# Completed	% Completed
Set8^{+/20}	51	51	100	51	100
Set8^{20/20}	54	0	0	1	1.9
Set8^{1/20}	50	41	82	50	100
1x Set8^{WT}	51	46	90	50	98
2x Set8^{WT}	53	51	96	48	90.5
1x Set8^{RG}	56	41	73	42	75
2x Set8^{RG}	47	36	76.5	43	91.4
1x Set8^{RGHL}	43	6	14	0	0
2x Set8^{RGHL}	44	28	63.6	17	38.6

Fig. 5. The *Set8^{RG}* mutant phenotype is not null. a) Pupation and b) Eclosion into adults of *Set8^{RG}* and *Set8^{RGHL}* mutants. Each circle represents the percentage of 40–50 larvae in a vial that reached pupation or adulthood. The mean and standard deviation of these percentages for 8 vials are shown for the indicated genotypes. Note that the Oregon-R and *Set8^{20/20}* data in panels (a) and (b) are identical to Fig. 2, b and c, respectively, and shown here to allow comparison. Significance was determined by a one-way ANOVA followed by Tukey’s multiple comparison test. P-values for pairwise comparisons can be found in Table 2 and Supplementary Table 3. c) Images of melanotic masses in *Set8^{RGHL}* and *Set8^{20/20}* third instar wandering larvae. Shown are two representative images for *Set8^{RGHL}* and one for *Set8^{20/20}*, with penetrance of the phenotype shown as a fraction and percentage below. Red circles indicate the location of the mass in each larva. d) SEM images of adult eyes of flies of the indicated genotypes. Penetrance and transgene copy number are as in Fig. 2 legend. e) Pupal length was measured for animals of the indicated genotypes. Each symbol represents a single pupa. Thick bar indicates the mean and thin bars indicate standard deviation. ns indicates not significant and **** indicates $P < 0.0001$ by a one-way ANOVA followed by Tukey’s multiple comparison test. f) Completion of anterior spiracle eversion and gas bubble translocation in *Set8* mutants and controls.

Table 2 Pairwise comparisons of pupation and eclosion frequencies among Set8 mutant genotypes

Genotype	Pupation frequency (%)	Eclosion frequency (%)		1	2	3	4	5	6	7	8
Oregon-R	0.91	0.90	1	Dark gray	ns	****	****	ns	****	****	****
Set8 ^{+/20}	0.87	0.83	2	ns	Dark gray	****	****	ns	****	****	****
Set8 ^{20/20}	0.66	0.00	3	****	****	Dark gray	****	****	ns	****	ns
Set8 ^{1/20}	0.88	0.45	4	ns	ns	****	Dark gray	****	****	ns	****
2x Set8 ^{WT}	0.91	0.94	5	ns	ns	****	ns	Dark gray	****	****	****
1x Set8 ^{RG}	0.82	0.00	6	ns	ns	**	ns	ns	Dark gray	****	ns
2x Set8 ^{RG}	0.90	0.45	7	ns	ns	****	ns	ns	ns	Dark gray	****
2x Set8 ^{RGHL}	0.84	0.00	8	ns	ns	**	ns	ns	ns	ns	Dark gray

Dark gray = pupation, light gray = eclosion;

****P < 0.0001,

**P < 0.01, ns = not significant

disparity further, we first generated H4^{K20R} mutants (Meers et al. 2018b) and compared the resulting phenotypes to those of both H4^{K20A} and Set8 mutants. Whereas a fraction of H4^{K20A} mutants can survive to adulthood, we found that all H4^{K20R} mutants fail to eclose as adults, although some reach the pharate adult stage (Fig. 6b and Table 3). In addition, H4^{K20R} animals pupate much less frequently than either H4^{K20A} mutants or HWT controls (Fig. 6c and Table 3). Notably, the H4^{K20R} mutant pupae are much smaller and shorter than either HWT control or H4^{K20A} mutant pupae, indicating a growth defect (Fig. 6, d and e). Despite this defect, we did not detect a change in cell cycle progression by FACS analysis of cells from H4^{K20R} wing imaginal discs (Fig. 6f). In contrast, H4^{K20A} cells accumulate in G2 relative to controls, with a concomitant reduction in S phase (Fig. 6f). Notably, Set8-deficient cells arrest in G2/M in both flies and mammalian cell culture (Karachentsev et al. 2005; Brustel et al. 2011). Taken together with the overall eclosion frequency differences, these data demonstrate that the H4^{K20R} mutation is more severe than the H4^{K20A} mutation developmentally, and that the developmental phenotypes of H4^{K20A}, H4^{K20R}, and Set8 mutants cannot be explained solely by effects on cell cycle progression.

One complication of these studies is that the fruit fly genome contains a single-copy replication-independent H4 gene (*His4r*) on chromosome 3 (i.e. located outside of the RD histone gene array on chromosome 2). *His4r* encodes an H4 protein that is identical to the RD H4 (Akhmanova et al. 1996). Although this gene is not essential (Fig. 6, b and c and Table 3), we and others have found that *His4r* can partially compensate for loss of RD H4 (McKay et al. 2015; Armstrong et al. 2018; Copur et al. 2018; Faragó et al. 2021). Therefore, we used CRISPR-Cas9 to engineer mutant *His4r* alleles [two deletions, *His4r*¹⁵⁻⁴ (Armstrong et al. 2018) and *His4r*^{S9} as well as a K20A mutant, *His4r*^{K20A}] and we combined them with the appropriate RD histone mutant genotypes (Fig. 6a). As shown in Fig. 6, b and c, homozygous loss of *His4r* in an H4^{K20A} background (H4^{K20A}, *His4r*^{Δ/Δ}) reduces viability, but does not eliminate it, indicating that *His4r* expression is important for the observed viability of H4^{K20A} mutants but is not required. Expressing one copy of *His4r*^{K20A} further reduces viability (Fig. 6, b and c and Table 3), suggesting a dominant toxicity of the H4K20A protein. In contrast, deleting *His4r* in an H4^{K20R} background did not appreciably change the lethal period of H4^{K20R} animals (Fig. 6, b and c and Table 3).

We next compared H4K20 and Set8 mutant phenotypes, focusing on pupariation and eye development. In contrast to Set8^{20/20} null mutants, which display defects during pupariation, >80% of the H4^{K20A} and H4^{K20R} animals complete proper anterior spiracle eversion and gas bubble translocation (Fig. 6h). Similarly, the viable Set8^{RG} and Set8^{1/20} mutants did not exhibit defects in anterior spiracle eversion or gas bubble translocation (Fig. 5f). Both Set8^{RG} and

Set8^{1/20} mutants have rough eyes (Fang et al. 2002) (Fig. 5d), indicating that Set8 is required for eye development. In contrast, none of the H4^{K20A} mutants had rough eyes when *His4r* was present, whereas ~21% of H4^{K20A}, *His4r*^{Δ/Δ} animals had only mild disorganization of interommatidial bristles (Fig. 6g). These results suggest that the roles of Set8 and H4K20me in eye development are distinct, and further highlight that the differential effects of Ala and Arg substitutions at H4^{K20}. We conclude that H4K20me does not mediate all functions of Set8 because mutating H4^{K20} and Set8 cause different developmental phenotypes.

Discussion

We used genetic approaches in *Drosophila* to investigate how histone PTMs, and the enzymes that install them, contribute to animal development. It is particularly informative to determine where these contributions differ. Our results indicate that only a subset of the essential functions of the H4K20 monomethyltransferase, Set8, are mediated by H4K20me. The data also reveal that H4K20me is formally dispensable for completion of development, although the lysine residue nonetheless plays an important role.

Drosophila Set8 and human KMT5A are orthologous

We showed that human KMT5A can substitute for all Set8 functions during *Drosophila* development, except in the eye, where we observe a minor disruption in ommatidial organization that manifests as a rough eye in KMT5A-rescued adults. The eye phenotype in KMT5A-rescued adults may not result from changes in methylation of substrates, as we found that the human KMT5A SET domain can fully substitute for that of Set8, even in the eye. In addition, we found that the rough eye phenotype was more penetrant in Set8^{AN}-rescued animals than it was in the KMT5A-rescued animals. Thus, full developmental eye function requires the non-catalytic amino terminal 339 amino acids of Set8, which are conserved in other Diptera, but not in humans or other vertebrates and invertebrates. One possible interpretation of these results is that some aspects of eye development do not require Set8 methyltransferase activity. However, Set8^{RG} catalytic mutants also display a rough eye phenotype. Consequently, an alternative interpretation is that the N-terminal domain directs Set8 to certain substrates important for eye development. Because KMT5A can perform nearly all the biological functions of Set8 in *Drosophila*, studies of Set8 could be applicable to human biology and disease, particularly because aberrant levels of KMT5A are implicated in the development of and increased risk in certain breast, brain, prostate, and liver cancers (Shi et al. 2007; Takawa et al. 2012; Yang et al. 2012; Dhami et al. 2013; Yu et al. 2013; Congdon et al. 2014; Yao et al. 2014; Nikolaou et al. 2015;

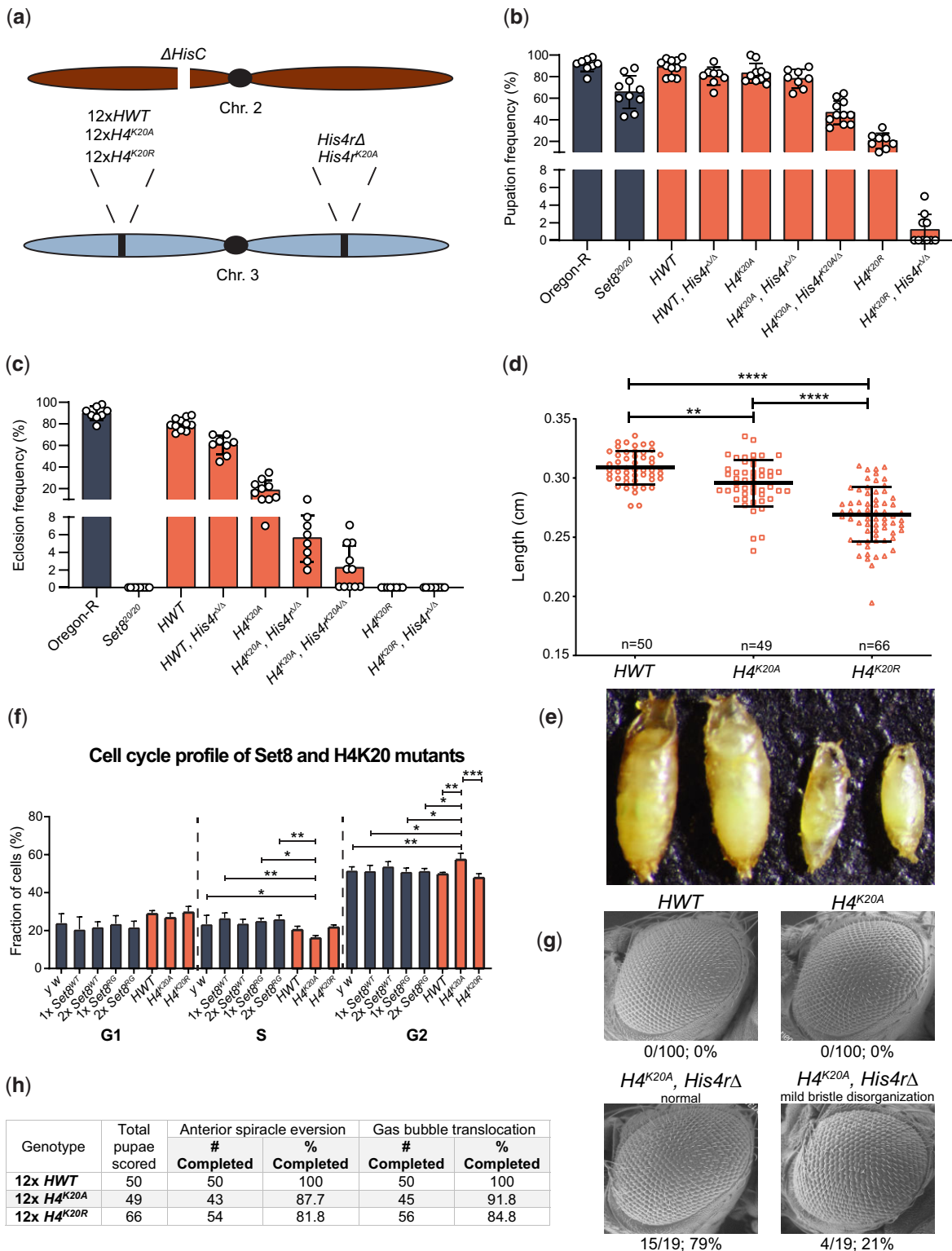


Fig. 6. H4K20 mutant phenotypes differ from Set8 mutant phenotypes. a) Diagram of histone mutant genotypes. A deletion of *HisC* on the second chromosome is rescued by a third chromosome containing a transgenic 12× histone gene arrays and either with or without a mutation of *His4r*. b) Pupation and c) eclosion into adults of different H4 mutants. Each circle represents the percentage of 40–50 larvae in a vial that reached pupation or adulthood. The mean and standard deviation of these percentages for 8–11 vials are shown for the indicated genotypes. Significance was determined by a one-way ANOVA followed by Tukey’s multiple comparison test. P-values for pairwise comparisons can be found in Table 3 and Supplementary Table 3. d) Pupal length was measured for animals of the indicated control and H4 genotypes. Each circle represents a single pupa. Thick bar indicates the mean and thin bars indicate standard deviation. ** indicates $P < 0.004$ and **** indicates $P < 0.0001$ by Student’s t test. e) Representative image used for the pupal length data in panel (e). f) FACS analysis of DNA content within cells obtained by dissociation of larval wing imaginal discs. The percentage of cells in each phase of interphase is shown for the indicated genotypes. g) SEM images of adult eyes of flies of HWT control and the indicated H4 mutant genotypes. Rough eye phenotype penetrance is indicated below each image. h) Completion of anterior spiracle eversion and gas bubble translocation in HWT, H4^{K20A}, and H4^{K20R}.

Table 3 Pairwise comparisons of pupation and eclosion frequencies among $H4^{K20A}$ mutant genotypes

Genotype	Pupation frequency (%)	Eclosion frequency (%)		1	2	3	4	5	6	7	8	9
Oregon-R	0.91	0.90	1	Dark gray	****	ns	****	****	****	****	****	****
Set8 ^{20/20}	0.66	0.00	2	****	Dark gray	****	****	****	ns	ns	ns	ns
HWT	0.89	0.80	3	ns	****	Dark gray	****	****	****	****	****	****
HWT, His4r ^{Δ/Δ}	0.81	0.60	4	ns	*	ns	Dark gray	****	****	****	****	****
H4 ^{K20A}	0.83	0.18	5	ns	***	ns	ns	Dark gray	*	****	****	****
H4 ^{K20A} , His4r ^{Δ/Δ}	0.77	0.06	6	ns	ns	ns	ns	ns	Dark gray	ns	ns	ns
H4 ^{K20A} , His4r ^{K20A/Δ}	0.45	0.02	7	****	****	****	****	****	****	Dark gray	ns	ns
H4 ^{K20R}	0.20	0.00	8	****	****	****	****	****	****	****	Dark gray	ns
H4 ^{K20R} , His4r ^{Δ/Δ}	0.01	0.00	9	****	****	****	****	****	****	****	****	Dark gray

Dark gray = pupation, light gray = eclosion;

**** $P < 0.0001$,

*** $P < 0.001$,

** $P < 0.01$,

* $P < 0.05$, ns = not significant

Milite et al. 2016; Zhang et al. 2016). Other recent studies implicate Set8 in neural stem cell reactivation (Huang et al. 2021), suggesting flies could also contribute to our understanding of neuronal function in humans.

Methyltransferase activity is important for the *in vivo* function of Set8

Whether methyltransferase activity is required for all the cellular and developmental roles of SET domain proteins remains an open question in the field, and cases where the catalytic activity of histone methyltransferases is not required for *in vivo* function have been described (Dorigi et al. 2017; Rickels et al. 2017). This question is generally addressed by testing the *in vivo* function of “catalytically dead” enzymes that contain a mutation in the SET domain. Previous *in vitro* studies showed that an R265G mutation eliminates catalytic activity of KMT5A (Fang et al. 2002; Nishioka et al. 2002). We found that the corresponding Set8^{R634G} mutation reduces but does not eliminate H4K20me1 and causes a hypomorphic rather than a null mutant phenotype resembling that of the previously described Set8¹ hypomorphic mutant (viable with rough eyes) (Fang et al. 2002; Karachentsev et al. 2005). Our structural analyses revealed that R634G disrupts interactions within the SAM binding domain but do not eliminate the possibility that SAM and K20 might still occupy the active site of the enzyme, albeit less avidly. The simplest interpretation of these data is that the R634G mutation impairs but does not eliminate Set8 methyltransferase activity, which is important for the *in vivo* function of Set8. Our observation that the Set8^{RGHL} mutant is genetically null and reduces H4K20me1 to the levels of a Set8 null mutant (i.e. very low or absent) is consistent with this interpretation. However, the Set8(RGHL) protein does not accumulate to control levels, confounding the straightforward conclusion that this mutant is null because of a lack of methyltransferase activity.

Comparative genetic analyses support distinct developmental roles for Set8 and H4K20me

Our analysis of $H4^{K20}$ mutants is consistent with the idea that Set8 provides essential functions during metazoan development that do not include H4K20 methylation. Animals entirely lacking H4K20me ($H4^{K20A}$, His4r^{Δ/Δ} and $H4^{K20A}$, His4r^{K20A/Δ}) can develop into adults with minimal morphological defects, whereas all animals lacking the Set8 H4K20 methyltransferase (Set8^{20/20}) die in early pupal stages. This difference in phenotype supports the hypothesis that Set8^{20/20} unviability is due, at least in part, to loss of non-histone substrate methylation and/or non-catalytic

functions of Set8. Nevertheless, $H4^{K20}$ is clearly quite important, as $H4^{K20R}$ mutants are inviable and only a small fraction of $H4^{K20A}$ mutants complete development and have increased levels of DNA damage in larval wing discs (Li et al. 2016). Moreover, ectopic expression of H4K20A mutant histones in cultured human cells supports a role for H4K20me in S phase progression, particularly in late replicating heterochromatin (Brustel et al. 2017).

The phenotypic differences we observe between $H4^{K20A}$ and $H4^{K20R}$ mutants are intriguing, as both substitutions are expected to eliminate H4K20me. The differences may well be attributable to idiosyncratic structural properties of H4A20- versus H4R20-containing nucleosomes, relative to wild-type. In particular, the side chains of Alanine and Arginine differ in both size and charge and thus may differentially impact interaction of the H4 tail with chromatin binding complexes irrespective of H4K20 methylation. For instance, proteins that bind unmethylated H4K20 (BRCA1-BARD1) do not recognize H4K20A nucleosomes (Nakamura et al. 2019). Given the proximity of H4K20 to the nucleosome core, these mutations may variably influence chromatin structure, or affect the modification of other residues on the H4 tail or on other histones within the nucleosome. Notably, the assumption that a Lys for Arg substitution would be less detrimental than a Lys for Ala substitution (because Lys and Arg have a similar side chain structure and are both positively charged) is not born out by our data. Regardless of the precise mechanism, our genetic analyses provide important insight into H4K20me function *in vivo*, and suggest that future biochemical, proteomic, and ultrastructural studies of these histone mutants will be informative.

Data availability

Strains and plasmids are available upon request. The authors affirm that all data necessary for confirming the conclusions of the article are present within the article, figures, and tables. Supplemental material is available on figshare: <https://doi.org/10.25386/genetics.19491587>.

Acknowledgments

The authors thank Ruth Steward for generously providing fly stocks and Megan Butler for critical reading of the manuscript.

Funding

ATC and RLA were supported in part by National Institutes of Health predoctoral traineeships, T32-GM007092. SK was supported in part by an National Institutes of Health diversity

supplement to grant R01-DA036897 (to RJD, AGM, and BDS) and by a postdoctoral traineeship, T32-CA009156. This work was supported by National Institutes of Health grants R35-GM126900 (to BDS), R35-GM136435 (to AGM), and R01-GM124201 (to RJD).

Conflicts of interest

None declared.

Literature cited

- Abbas T, Mueller AC, Shibata E, Keaton M, Rossi M, Dutta A. CRL1-FBXO11 promotes Cdt2 ubiquitylation and degradation and regulates Pr-Set7/Set8-mediated cellular migration. *Mol Cell*. 2013;49(6):1147–1158.
- Abbas T, Shibata E, Park J, Jha S, Karnani N, Dutta A. CRL4Cdt2 regulates cell proliferation and histone gene expression by targeting PR-Set7/Set8 for degradation. *Mol Cell*. 2010;40(1):9–21.
- Akhmanova A, Miedema K, Hennig W. Identification and characterization of the *Drosophila* histone H4 replacement gene. *FEBS Lett*. 1996;388(2–3):219–222.
- Armstrong RL, Penke TJR, Chao SK, Gentile GM, Strahl BD, Matera AG, McKay DJ, Duronio RJ. H3K9 promotes under-replication of pericentromeric heterochromatin in *Drosophila* salivary gland polytene chromosomes. *Genes (Basel)*. 2019;10(2):93.
- Armstrong RL, Penke TJR, Strahl BD, Matera AG, McKay DJ, MacAlpine DM, Duronio RJ. Chromatin conformation and transcriptional activity are permissive regulators of DNA replication initiation in *Drosophila*. *Genome Res*. 2018;28(11):1688–1700.
- Baker NE, Li K, Quiquand M, Ruggiero R, Wang LH. Eye development. *Methods*. 2014;68(1):252–259.
- Bateman JR, Larschan E, D'Souza R, Marshall LS, Dempsey KE, Johnson JE, Mellone BG, Kuroda MI. A genome-wide screen identifies genes that affect somatic homolog pairing in *Drosophila*. *G3 (Bethesda)*. 2012;2(7):731–740.
- Beck DB, Burton A, Oda H, Ziegler-Birling C, Torres-Padilla M-E, Reinberg D. The role of PR-Set7 in replication licensing depends on Suv4-20h. *Genes Dev*. 2012a;26(23):2580–2589.
- Beck DB, Oda H, Shen SS, Reinberg D. PR-set7 and H4K20me1: at the crossroads of genome integrity, cell cycle, chromosome condensation, and transcription. *Genes Dev*. 2012b;26(4):325–337.
- Blazer LL, Lima-Fernandes E, Gibson E, Eram MS, Loppnau P, Arrowsmith CH, Schapira M, Vedadi M. PR domain-containing protein 7 (PRDM7) is a histone 3 lysine 4 trimethyltransferase. *J Biol Chem*. 2016;291(26):13509–13519.
- Bodenhofer U, Bonatesta E, Horejš-Kainrath C, Hochreiter S. msa: an R package for multiple sequence alignment. *Bioinformatics*. 2015;31(24):3997–3999.
- Botuyan MV, Lee J, Ward IM, Kim J-E, Thompson JR, Chen J, Mer G. Structural basis for the methylation state-specific recognition of histone H4-K20 by 53BP1 and Crb2 in DNA repair. *Cell*. 2006;127(7):1361–1373.
- Brustel J, Kirstein N, Izard F, Grimaud C, Prorok P, Cayrou C, Schotta G, Abdelsamie AF, Déjardin J, Méchali M, et al. Histone H4K20 trimethylation at late-firing origins ensures timely heterochromatin replication. *EMBO J*. 2017;36(18):2726–2741.
- Brustel J, Tardat M, Kirsh O, Grimaud C, Julien E. Coupling mitosis to DNA replication: the emerging role of the histone H4-lysine 20 methyltransferase PR-Set7. *Trends Cell Biol*. 2011;21(8):452–460.
- Case DA, Ben-Shalom IY, Brozell SR, Cerutti DS, Cheatham TE, III, Cruzeiro VWD, Darden TA, Duke RE, Ghoreishi D, Gilson MK, et al. Amber 2018. Univ California, San Francisco. 2018:1–923.
- Centore RC, Havens CG, Manning AL, Li J-M, Flynn RL, Tse A, Jin J, Dyson NJ, Walter JC, Zou L. CRL4Cdt2-mediated destruction of the histone methyltransferase Set8 prevents premature chromatin compaction in S phase. *Mol Cell*. 2010;40(1):22–33.
- Chamberlain SA, Szöcs E. Taxize: taxonomic search and retrieval in R. *F1000Res*. 2013;2:191.
- Congdon LM, Houston SI, Veerappan CS, Spektor TM, Rice JC. PR-Set7-mediated monomethylation of histone H4 lysine 20 at specific genomic regions induces transcriptional repression. *J Cell Biochem*. 2010;110(3):609–619.
- Congdon LM, Sims JK, Tuzon CT, Rice JC. The PR-Set7 binding domain of Riz1 is required for the H4K20me1-H3K9me1 trans-tail “histone code” and Riz1 tumor suppressor function. *Nucleic Acids Res*. 2014;42(6):3580–3589.
- Copur Ö, Gorchakov A, Finkl K, Kuroda MI, Müller J. Sex-specific phenotypes of histone H4 point mutants establish dosage compensation as the critical function of H4K16 acetylation in *Drosophila*. *Proc Natl Acad Sci U S A*. 2018;115(52):13336–13341.
- Cornett EM, Ferry L, Defossez PA, Rothbart SB. Lysine methylation regulators moonlighting outside the epigenome. *Mol Cell*. 2019;75(6):1092–1101.
- Couture JF, Collazo E, Brunzelle JS, Trievel RC. Structural and functional analysis of SET8, a histone H4 Lys-20 methyltransferase. *Genes Dev*. 2005;19(12):1455–1465.
- Dhami GK, Liu H, Galka M, Voss C, Wei R, Muranko K, Kaneko T, Cregan SP, Li L, Li SSC. Dynamic methylation of numb by Set8 regulates its binding to p53 and apoptosis. *Mol Cell*. 2013;50(4):565–576.
- Dillon SC, Zhang X, Trievel RC, Cheng X. The SET-domain protein superfamily: protein lysine methyltransferases. *Genome Biol*. 2005;6(8):227.
- Dorigi KM, Swigut T, Henriques T, Bhanu NV, Scruggs BS, Nady N, Still CD, Garcia BA, Adelman K, Wysocka J. Mll3 and Mll4 facilitate enhancer RNA synthesis and transcription from promoters independently of H3K4 monomethylation. *Mol Cell*. 2017;66(4):568–576.e4.
- Dulev S, Tkach J, Lin S, Batada NN. SET 8 methyltransferase activity during the DNA double-strand break response is required for recruitment of 53 BP 1. *EMBO Rep*. 2014;15(11):1163–1174.
- Fang J, Feng Q, Ketel CS, Wang H, Cao R, Xia L, Erdjument-Bromage H, Tempst P, Simon JA, Zhang Y. Purification and functional characterization of SET8, a nucleosomal histone H4-Lysine 20-specific methyltransferase. *Curr Biol*. 2002;12(13):1086–1099.
- Faragó A, Ürmösi A, Farkas A, Bodai L. The histone replacement gene *His4r* is involved in heat stress induced chromatin rearrangement. *Sci Rep*. 2021;11(1):1–15.
- Fumasoni I, Meani N, Rambaldi D, Scafetta G, Alcalay M, Ciccarelli FD. Family expansion and gene rearrangements contributed to the functional specialization of PRDM genes in vertebrates. *BMC Evol Biol*. 2007;7(1):1–11.
- Götz AW, Williamson MJ, Xu D, Poole D, Le Grand S, Walker RC. Routine microsecond molecular dynamics simulations with AMBER on GPUs. 1. Generalized born. *J Chem Theory Comput*. 2012;8(5):1542–1555.
- Günesdogan U, Jäckle H, Herzig A. A genetic system to assess in vivo the functions of histones and histone modifications in higher eukaryotes. *EMBO Rep*. 2010;11(10):772–776.
- Hamidi T, Singh AK, Veland N, Vemulapalli V, Chen J, Hardikar S, Bao J, Fry CJ, Yang V, Lee KA, et al. Identification of Rpl29 as a major substrate of the lysine methyltransferase Set7/9. *J Biol Chem*. 2018;293(33):12770–12780.
- Hayashi-Takanaka Y, Hayashi Y, Hirano Y, Miyawaki-Kuwakado A, Ohkawa Y, Obuse C, Kimura H, Haraguchi T, Hiraoka Y.

- Chromatin loading of MCM hexamers is associated with di-/tri-methylation of histone H4K20 toward S phase entry. *Nucleic Acids Res.* 2021;49(21):12152–12166.
- Houston SI, McManus KJ, Adams MM, Sims JK, Carpenter PB, Hendzel MJ, Rice JC. Catalytic function of the PR-Set7 histone H4 lysine 20 monomethyltransferase is essential for mitotic entry and genomic stability. *J Biol Chem.* 2008;283(28):19478–19488.
- Huang J, Gujar MR, Deng Q, Chia SY, Li S, Tan P, Sung W, Wang H. Histone lysine methyltransferase Pr-set7/SETD8 promotes neural stem cell reactivation. *EMBO Rep.* 2021;22(4):e50994.
- Huen MSY, Sy SM-H, van Deursen JM, Chen J. Direct interaction between SET8 and proliferating cell nuclear antigen couples H4-K20 methylation with DNA replication. *J Biol Chem.* 2008;283(17):11073–11077.
- Jiang F, Liu Q, Wang Y, Zhang J, Wang H, Song T, Yang M, Wang X, Kang L. Comparative genomic analysis of SET domain family reveals the origin, expansion, and putative function of the arthropod-specific SmydA genes as histone modifiers in insects. *Gigascience.* 2017;6(6):1–16.
- Jørgensen S, Elvers I, Trelle MB, Menzel T, Eskildsen M, Jensen ON, Helleday T, Helin K, Sørensen CS. The histone methyltransferase SET8 is required for S-phase progression. *J Cell Biol.* 2007;179(7):1337–1345.
- Julien E, Herr W. A switch in mitotic histone H4 lysine 20 methylation status is linked to M phase defects upon loss of HCF-1. *Mol Cell.* 2004;14(6):713–725.
- Kalakonda N, Fischle W, Boccuni P, Gurvich N, Hoya-Arias R, Zhao X, Miyata Y, MacGrogan D, Zhang J, Sims JK, et al. Histone H4 lysine 20 monomethylation promotes transcriptional repression by L3MBTL1. *Oncogene.* 2008;27(31):4293–4304.
- Kapoor-Vazirani P, Vertino PM. A dual role for the histone methyltransferase PR-SET7/SETD8 and histone H4 lysine 20 monomethylation in the local regulation of RNA polymerase II pausing. *J Biol Chem.* 2014;289(11):7425–7437.
- Karachentsev D, Sarma K, Reinberg D, Steward R. PR-Set7-dependent methylation of histone H4 Lys 20 functions in repression of gene expression and is essential for mitosis. *Genes Dev.* 2005;19(4):431–435.
- Leatham-Jensen M, Uyehara CM, Strahl BD, Matera AG, Duronio RJ, McKay DJ. Lysine 27 of replication-independent histone H3.3 is required for Polycomb target gene silencing but not for gene activation. *PLoS Genet.* 2019;15(1):e1007932.
- Li Y, Armstrong RL, Duronio RJ, Macalpine DM. Methylation of histone H4 lysine 20 by PR-Set7 ensures the integrity of late replicating sequence domains in *Drosophila*. *Nucleic Acids Res.* 2016;44(15):7204–7218.
- Li Y, Sun L, Zhang Y, Wang D, Wang F, Liang J, Gui B, Shang Y. The histone modifications governing TFF1 transcription mediated by estrogen receptor. *J Biol Chem.* 2011a;286(16):13925–13936.
- Li Z, Nie F, Wang S, Li L. Histone H4 Lys 20 monomethylation by histone methylase SET8 mediates Wnt target gene activation. *Proc Natl Acad Sci U S A.* 2011b;108(8):3116–3123.
- Lukinović V, Casanova AG, Roth GS, Chuffart F, Reynoird N. Lysine methyltransferases signaling: histones are just the tip of the iceberg. *Curr Protein Pept Sci.* 2020;21(7):655–674.
- Lv X, Han Z, Chen H, Yang B, Yang X, Xia Y, Pan C, Fu L, Zhang S, Han H, et al. A positive role for polycomb in transcriptional regulation via H4K20me1. *Cell Res.* 2016;26(5):529–542.
- Maier JA, Martinez C, Kasavajhala K, Wickstrom L, Hauser KE, Simmerling C. ff14SB: improving the accuracy of protein side chain and backbone parameters from ff99SB. *J Chem Theory Comput.* 2015;11(8):3696–3713.
- Manes G, Joly W, Guignard T, Smirnov V, Berthemy S, Bocquet B, Audo I, Zeitz C, Sahel J, Cazevielle C, et al. A novel duplication of PRMD13 causes North Carolina macular dystrophy: overexpression of PRDM13 orthologue in *Drosophila* eye reproduces the human phenotype. *Hum Mol Genet.* 2017;26(22):4367–4374.
- McKay DJ, Klusza S, Penke TJR, Meers MP, Curry KP, McDaniel SL, Malek PY, Cooper SW, Tatomer DC, Lieb JD, et al. Interrogating the function of metazoan histones using engineered gene clusters. *Dev Cell.* 2015;32(3):373–386.
- Meers MP, Adelman K, Duronio RJ, Strahl BD, McKay DJ, Matera AG. Transcription start site profiling uncovers divergent transcription and enhancer-associated RNAs in *Drosophila melanogaster*. *BMC Genomics* 2018 191. 2018a;19(1):1–20.
- Meers MP, Henriques T, Lavender CA, McKay DJ, Strahl BD, Duronio RJ, Adelman K, Matera AG. Histone gene replacement reveals a posttranscriptional role for H3K36 in maintaining metazoan transcriptome fidelity. *Elife.* 2017;6:e23249.
- Meers MP, Leatham-Jensen M, Penke TJR, McKay DJ, Duronio RJ, Matera AG. An animal model for genetic analysis of multi-gene families: cloning and transgenesis of large tandemly repeated histone gene clusters. *Methods Mol Biol.* 2018b;1832:309–325.
- Meserve JH, Duronio RJ. A population of G2-arrested cells are selected as sensory organ precursors for the interommatidial bristles of the *Drosophila* eye. *Dev Biol.* 2017;430(2):374–384.
- Milite C, Feoli A, Viviano M, Rescigno D, Cianciulli A, Balzano AL, Mai A, Castellano S, Sbardella G. The emerging role of lysine methyltransferase SETD8 in human diseases. *Clin Epigenet.* 2016;8(1):1–11.
- Minakhina S, Steward R. Melanotic mutants in *Drosophila*: pathways and phenotypes. *Genetics.* 2006;174(1):253–263.
- Mis J, Ner SS, Grigliatti TA. Identification of three histone methyltransferases in *Drosophila*: dG9a is a suppressor of PEV and is required for gene silencing. *Mol Genet Genomics.* 2006;275(6):513–526.
- Mohan M, Herz H-M, Smith ER, Zhang Y, Jackson J, Washburn MP, Florens L, Eissenberg JC, Shilatifard A. The COMPASS family of H3K4 methylases in *Drosophila*. *Mol Cell Biol.* 2011;31(21):4310–4318.
- Nakamura K, Saredi G, Becker JR, Foster BM, Nguyen NV, Beyer TE, Cesa LC, Faull PA, Lukauskas S, Frimurer T, et al. H4K20me0 recognition by BRCA1–BARD1 directs homologous recombination to sister chromatids. *Nat Cell Biol.* 2019;21(3):311–318.
- Nikolaou KC, Moulos P, Chalepakis G, Hatzis P, Oda H, Reinberg D, Talianidis I. Spontaneous development of hepatocellular carcinoma with cancer stem cell properties in PR-SET7-deficient livers. *EMBO J.* 2015;34(4):430–447.
- Nishioka K, Rice JC, Sarma K, Erdjument-Bromage H, Werner J, Wang Y, Chuikov S, Valenzuela P, Tempst P, Steward R, et al. PR-Set7 is a nucleosome-specific methyltransferase that modifies lysine 20 of histone H4 and is associated with silent chromatin. *Mol Cell.* 2002;9(6):1201–1213.
- Oda H, Hübner MR, Beck DB, Vermeulen M, Hurwitz J, Spector DL, Reinberg D. Regulation of the histone H4 monomethylase PR-Set7 by CRL4Cdt2-mediated PCNA-dependent degradation during DNA damage. *Mol Cell.* 2010;40(3):364–376.
- Oda H, Okamoto I, Murphy N, Chu J, Price SM, Shen MM, Torres-Padilla M-E, Heard E, Reinberg D. Monomethylation of histone H4-lysine 20 is involved in chromosome structure and stability and is essential for mouse development. *Mol Cell Biol.* 2009;29(8):2278–2295.
- Pannetier M, Julien E, Schotta G, Tardat M, Sardet C, Jenuwein T, Feil R. PR-SET7 and SUV4-20H regulate H4 lysine-20 methylation at imprinting control regions in the mouse. *EMBO Rep.* 2008;9(10):998–1005.

- Penke TJR, McKay DJ, Strahl BD, Matera AG, Duronio RJ. Direct interrogation of the role of H3K9 in metazoan heterochromatin function. *Genes Dev.* 2016;30(16):1866–1880.
- Penke TJR, McKay DJ, Strahl BD, Matera AG, Duronio RJ. Functional redundancy of variant and canonical histone H3 lysine 9 modification in *Drosophila*. *Genetics.* 2018;208(1):229–244.
- Pesavento JJ, Yang H, Kelleher NL, Mizzen CA. Certain and progressive methylation of histone H4 at lysine 20 during the cell cycle. *Mol Cell Biol.* 2008;28(1):468–486.
- Rickels R, Herz H-M, Sze CC, Cao K, Morgan MA, Collings CK, Gause M, Takahashi YH, Wang L, Rendleman EJ, et al. Histone H3K4 monomethylation catalyzed by Trr and mammalian COMPASS-like proteins at enhancers is dispensable for development and viability. *Nat Genet.* 2017;49(11):1647–1653.
- Rothbart SB, Strahl BD. Interpreting the language of histone and DNA modifications. *Biochim Biophys Acta.* 2014;1839(8):627–643.
- Sakaguchi A, Joyce E, Aoki T, Schedl P, Steward R. The histone H4 lysine 20 monomethyl mark, set by PR-Set7 and stabilized by L(3)mbt, is necessary for proper interphase chromatin organization. *PLoS One.* 2012;7(9):e45321.
- Sakaguchi A, Karachentsev D, Seth-Pasricha M, Druzhinina M, Steward R. Functional characterization of the *Drosophila* Hmt4-20/Suv4-20 histone methyltransferase. *Genetics.* 2008;179(1):317–322.
- Sakaguchi A, Steward R. Aberrant monomethylation of histone H4 lysine 20 activates the DNA damage checkpoint in *Drosophila melanogaster*. *J Cell Biol.* 2007;176(2):155–162.
- Salomon-Ferrer R, Götz AW, Poole D, Le Grand S, Walker RC. Routine microsecond molecular dynamics simulations with AMBER on GPUs. 2. Explicit solvent particle mesh ewald. *J Chem Theory Comput.* 2013;9(9):3878–3888.
- Schotta G, Lachner M, Sarma K, Ebert A, Sengupta R, Reuter G, Reinberg D, Jenuwein T. A silencing pathway to induce H3-K9 and H4-K20 trimethylation at constitutive heterochromatin. *Genes Dev.* 2004;18(11):1251–1262.
- Schotta G, Sengupta R, Kubicek S, Malin S, Kauer M, Callén E, Celeste A, Pagani M, Opravil S, De La Rosa-Velazquez IA, et al. A chromatin-wide transition to H4K20 monomethylation impairs genome integrity and programmed DNA rearrangements in the mouse. *Genes Dev.* 2008;22(15):2048–2061.
- Shi X, Kachirskaja I, Yamaguchi H, West LE, Wen H, Wang EW, Dutta S, Appella E, Gozani O. Modulation of p53 function by SET8-mediated methylation at lysine 382. *Mol Cell.* 2007;27(4):636–646.
- Shilatifard A. The COMPASS family of histone H3K4 methylases: mechanisms of regulation in development and disease pathogenesis. *Annu Rev Biochem.* 2012;81:65–95.
- Shoib M, Chen Q, Shi X, Nair N, Prasanna C, Yang R, Walter D, Frederiksen KS, Einarsson H, Svensson JP, et al. Histone H4 lysine 20 mono-methylation directly facilitates chromatin openness and promotes transcription of housekeeping genes. *Nat Commun.* 2021;12(1):1–16.
- Shoib M, Walter D, Gillespie PJ, Izard F, Fahrenkrog B, Lleres D, Lerdrup M, Johansen JV, Hansen K, Julien E, et al. Histone H4K20 methylation mediated chromatin compaction threshold ensures genome integrity by limiting DNA replication licensing. *Nat Commun.* 2018;9(1):3704.
- Sims JK, Rice JC. PR-Set7 establishes a repressive trans-tail histone code that regulates differentiation. *Mol Cell Biol.* 2008;28(14):4459–4468.
- Spektor TM, Congdon LM, Veerappan CS, Rice JC. The UBC9 E2 sumo conjugating enzyme binds the PR-Set7 histone methyltransferase to facilitate target gene repression. *PLoS One.* 2011;6(7):e22785.
- Sugeedha J, Gautam J, Tyagi S. SET1/MLL family of proteins: functions beyond histone methylation. *Epigenetics.* 2021;16(5):469–487.
- Takawa M, Cho HS, Hayami S, Toyokawa G, Kogure M, Yamane Y, Iwai Y, Maejima K, Ueda K, Masuda A, et al. Histone lysine methyltransferase setd8 promotes carcinogenesis by deregulating PCNA expression. *Cancer Res.* 2012;72(13):3217–3227.
- Tardat M, Brustel J, Kirsh O, Lefevbre C, Callanan M, Sardet C, Julien E. The histone H4 Lys 20 methyltransferase PR-Set7 regulates replication origins in mammalian cells. *Nat Cell Biol.* 2010;12(11):1086–1093.
- Tardat M, Murr R, Herceg Z, Sardet C, Julien E. PR-Set7-dependent lysine methylation ensures genome replication and stability through S phase. *J Cell Biol.* 2007;179(7):1413–1426.
- Thandapani P, Couturier AM, Yu Z, Li X, Couture JF, Li S, Masson JY, Richard S. Lysine methylation of FEN1 by SET7 is essential for its cellular response to replicative stress. *Oncotarget.* 2017;8(39):64918–64931.
- Tullio FD, Schwarz M, Zorgati H, Mzoughi S, Guccione E. The duality of PRDM proteins: epigenetic and structural perspectives. *FEBS J.* 2021;289(5):1256–1275. doi:10.1111/febs.15844.
- Wakabayashi K, Okamura M, Tsutsumi S, Nishikawa NS, Tanaka T, Sakakibara I, Kitakami J, Ihara S, Hashimoto Y, Hamakubo T, et al. The peroxisome proliferator-activated receptor/retinoid X receptor heterodimer targets the histone modification enzyme PR-Set7/Setd8 gene and regulates adipogenesis through a positive feedback loop. *Mol Cell Biol.* 2009;29(13):3544–3555.
- Wang H, Cao R, Xia L, Erdjument-Bromage H, Borchers C, Tempst P, Zhang Y. Purification and functional characterization of a histone H3-lysine 4-specific methyltransferase. *Mol Cell.* 2001;8(6):1207–1217.
- Weirich S, Kudithipudi S, Jeltsch A. Specificity of the SUV4-20H1 and SUV4-20H2 protein lysine methyltransferases and methylation of novel substrates. *J Mol Biol.* 2016;428(11):2344–2358.
- West LE, Roy S, Lachmi-Weiner K, Hayashi R, Shi X, Appella E, Kutateladze TG, Gozani O. The MBT repeats of L3MBTL1 link SET8-mediated p53 methylation at lysine 382 to target gene repression. *J Biol Chem.* 2010;285(48):37725–37732.
- Wolff T, Ready DF. The beginning of pattern formation in the *Drosophila* compound eye: the morphogenetic furrow and the second mitotic wave. *Development.* 1991;113(3):841–850.
- Wu S, Rice JC. A new regulator of the cell cycle: the PR-Set7 histone methyltransferase. *Cell Cycle.* 2011;10(1):68–72.
- Wu S, Wang W, Kong X, Congdon LM, Yokomori K, Kirschner MW, Rice JC. Dynamic regulation of the PR-Set7 histone methyltransferase is required for normal cell cycle progression. *Genes Dev.* 2010;24(22):2531–2542.
- Yang F, Sun L, Li Q, Han X, Lei L, Zhang H, Shang Y. SET8 promotes epithelial-mesenchymal transition and confers TWIST dual transcriptional activities. *EMBO J.* 2012;31(1):110–123.
- Yang H, Pesavento JJ, Starnes TW, Cryderman DE, Wallrath LL, Kelleher NL, Mizzen CA. Preferential dimethylation of histone H4 lysine 20 by Suv4-20. *J Biol Chem.* 2008;283(18):12085–12092.
- Yao L, Li Y, Du F, Han X, Li X, Niu Y, Ren S, Sun Y. Histone H4 Lys 20 methyltransferase SET8 promotes androgen receptor-mediated transcription activation in prostate cancer. *Biochem Biophys Res Commun.* 2014;450(1):692–696.
- Yin Y, Yu VC, Zhu G, Chang DC, Yin L, Yu VC, Zhu G, Chang DC. SET8 plays a role in controlling G₁/S transition by blocking lysine acetylation in histone through binding to H4 N-terminal tail. *Cell Cycle.* 2008;7(10):1423–1432.
- Yu G. Using ggtree to visualize data on tree-like structures. *Curr Protoc Bioinforma.* 2020;69(1):e96.

- Yu G, Lam TTY, Zhu H, Guan Y. Two methods for mapping and visualizing associated data on phylogeny using ggtree. *Mol Biol Evol.* 2018;35(12):3041–3043.
- Yu G, Smith DK, Zhu H, Guan Y, Lam TTY. ggtree: an r package for visualization and annotation of phylogenetic trees with their covariates and other associated data. *Methods Ecol Evol.* 2017;8(1):28–36.
- Yu N, Huangyang P, Yang X, Han X, Yan R, Jia H, Shang Y, Sun L. microRNA-7 suppresses the invasive potential of breast cancer cells and sensitizes cells to DNA damages by targeting histone methyltransferase SET8. *J Biol Chem.* 2013;288(27):19633–19642.
- Yu Y, Liu L, Li X, Hu X, Song H. The histone H4K20 methyltransferase PR-Set7 fine-tunes the transcriptional activation of Wingless signaling in *Drosophila*. *J Genet Genomics.* 2019;46(1):57–59.
- Zhang J, Hou W, Chai M, Zhao H, Jia J, Sun X, Zhao B, Wang R. MicroRNA-127-3p inhibits proliferation and invasion by targeting SETD8 in human osteosarcoma cells. *Biochem Biophys Res Commun.* 2016;469(4):1006–1011.
- Zhang X, Huang Y, Shi X. Emerging roles of lysine methylation on non-histone proteins. *Cell Mol Life Sci.* 2015;72(22):4257–4272.
- Zouaz A, Fernando C, Perez Y, Sardet C, Julien E, Grimaud C. Cell-cycle regulation of non-enzymatic functions of the *Drosophila* methyltransferase PR-Set7. *Nucleic Acids Res.* 2018;46(6):2834–2849.

Communicating editor: B. Calvi